UNIVERSIDAD TECNICA
FEDERICO SANTA MARIA

INSA INSTITUT NATIONAL DES SCIENCES APPLIQUÉES LYON

sarrasola

VINCI ENERGIES

Undergraduate Final Project

Modal shape analysis applied to Non-Destructive Testing on metallic towers

September 2021



Student: Charline Garcelon

Mechanical Engineering Dual Degree Program

Advisors: Alejandro Pacheco Sanjuán (UTFSM), **Simon Chesne** (INSA Lyon), **Eric Marin** (Sarrasola)

Abstract

Metallic towers are continually exposed to environmental conditions such as humidity and wind which make them prone to corrosion problems after a prolonged exposure. As a results, localized brittle portions of corroded material form over time weakening the global stability of the structure. Visual inspections reveal that these brittle spots are located mostly at connections between mast sections and ground foundation.

The objective of the present work is to investigate a non-destructive technique based on modal shape analysis to assess the current global structural condition of metallic towers. This research work was performed by the author during an internship in Sarrasola company (VINCI Energies group) within the context of an end-of-studies industrial experience.

Two campaigns of vibratory experiments were performed: one with a ski-lift tower (not linked to a line) and one with a power-line tower (linked to uncharged electric cables). Different types of sensors and perturbations were utilized for data collection: 3D-velocimeters with ambient noise excitation, 3D-MEMS accelerometers with ambient noise excitation, and piezoelectric accelerometers with shock perturbation. Sensors were fixed along the mast and synchronized to record the global behavior (overall motion) in each structure. As a general trend it was observed that vibration modes occur at low frequencies, between 1 and 20 Hz.

Several configurations of boundary conditions were tested on the ski-lift tower to determine which kind of defects would be identified with such arrangement of sensors. In particular, the following configurations were tested: half of the anchoring rods unbolted along with one side and two sides weights (1300 daN) applied on the top of the tower.

A Fast Fourier Transform (FFT) based code was developed to process velocity recordings in the commercial software MATLAB. This code provides the natural frequencies of each tower and also the

deformed shape related to each mode. In addition, a complete CAD model of the ski-lift tower was built in Autodesk software to obtain a numerical estimate of its mode shapes by using the Finite Element Method.

The tested ski-lift tower was not exactly set in normal operating conditions since it was not linked to a cable line.

As a consequence, the recorded velocity signals were clean, so it was possible to clearly identify up to five modes of vibrations (four bending modes and one torsion mode) with their frequencies and corresponding deformed shapes. The first bending modes were identified at 3.02 and 11.37Hz in longitudinal direction (along the cable line) and 2.79Hz and 11.98Hz in transversal direction. The measured deformed shapes for these modes were very close to the numerical results. The first torsional mode was observed at 6.54Hz.

When half of the foundation bolts were removed the frequency of the first mode decreased by 45%. This effect was counteracted in the case where the mast was strongly tensed by cables. It was observed that the directions of the mode shapes were diverted from the tower symmetry planes and also the appearance of new secondary frequency peaks.

The tested tower was a lattice structure connected to a power line with cables. The recorded raw signals were quite noisy, so it was difficult to identify precisely the frequency of the mode shape among several peaks closed to each other. In this case natural frequencies were determined with an accuracy of 0.5 Hz. Such frequency peak distribution might be the result of resonance in the cable line. The measured natural frequencies were 3.8Hz and 9.2Hz for the first longitudinal bending modes, and 2.9Hz and 8.4Hz for the first transversal bending modes. Despite that the exact natural frequencies could not be assessed with confidence, the signal corresponded to almost the same deformed shape for the different frequency peaks close to each other. These shapes were consistent with the numerically predicted deformed shapes.

Key words: Ski-lift tower, power-line tower, Non-Destructive Technique, vibrations, mode shapes, resonance, ambient noise, velocimeters.

Acknowledgements

Je remercie l'entreprise Sarrasola et tous ses collaborateurs pour m'avoir accueillie avec bienveillance dans les locaux de Grésy.

J'adresse une mention particulière à Eric Marin qui m'a choisie pour intégrer cette aventure et surtout m'a accompagnée et épaulée durant ces six mois. Sa créativité et son recul m'ont permis d'appréhender les aléas du monde de la recherche.

Quiero agradecer luego a mi profesor tutor Alejandro Pacheco por siempre recordarme el espíritu de la investigación, no admitiendo sino demostrando, y también por hacerme sentir que sí, soy capaz.

Je remercie Simon Chesne et Adrien Marswick pour leur appui technique et pour avoir assuré la continuité entre mon stage et les travaux de recherches antérieurs sur le sujet.

Merci à l'INSA de Lyon pour ses formations techniques de qualité, notamment en termes de travaux pratiques où l'on m'a toujours fait tant confiance.

Agradezco a la Universidad Técnica Féderico Santa Maria por recibirme en su hermoso campus de excelencia y por darme la oportunidad de atender clases cuya matrería se expande más allá de lo técnico.

Enfin, merci à Emmanuel Mignot pour avoir porté ce projet de double-diplôme entre l'INSA et l'USM en insistant sur l'intérêt du stage en entreprise, lequel m'a semblé véritablement complémentaire avec les enseignements académiques dispensés.

Index

1. Introduction 7

1.1. Critical issues on metallic towers 7

1.2. Problem statement 7

1.3. Key objectives and specific targets 8

1.4. Scope of the investigation 9

2. Theoretical background 10

2.1. Resonance phenomenon 10

2.2. Analytic dynamic approach 11

2.3. Lagrange equations approach 12

2.4. Analytic resolution 13

2.5. Generalization to N-DOF system 16

2.6. Theoretical Transfer Function 16

2.7. Experimental approach 20

3. Literature review 25

3.1. Visual inspection 25

3.2. Dye penetrant inspection (DP) 25

3.3. Ultrasonic Testing (UT) 26

3.4. Eddy Current Testing (ECT) 28

3.5. Modal analysis 30

4. Methodology 37

4.1. Measurements 37

4.3. Post-processing 45

4.4. Geometry capture 48

4.5. Numerical model 50

5. Results and analysis 53

5.1. Ski-lift tower *53*

5.2. Powerline tower *58*

5.3. Signal distortion *62*

6. Conclusions 71

6.1. Technical conclusions *71*

6.2. Perspectives and future work *72*

6.3. Personal experience *75*

7. Bibliography 76

7.1. Theoretical basics *76*

7.2. State of the art *78*

7.3. Vibration analysis Applied to concrete cases *79*

7.4. Internal documentation *80*

8. Appendix 81

1. Introduction

1.1. Critical issues on metallic towers

Most of the current power grids, ski-lift tower networks and wind farms currently operating in Europe were built in the 20th century. All these structures are getting old nowadays, so that structural failures can occur, putting people's life at risk or shutting down electrical production for days.

The most common failures in such tower masts are due to corrosion, or eventually to weld fractures. Generally, when such flaws are visible with the naked eye, it means the structure is already in a critical state. Besides, the towers are used to be painted to, precisely, avoid corrosion, but it makes the defects harder to detect in time, hidden behind this coat of paint.

Another possible degradation across the time is the lack of fatigue resistance of the foundation. For ski-lift tower or wind turbines, the rod anchors and the concrete basement need to be sufficiently dimensioned to handle the dissymmetric applied loads. Landslides can also weaken this robustness.

1.2. Problem statement

The operators are thinking more and more about repairing or renewing part of their grid. However, they cannot renew all of it at once for obvious financial and logistical reasons. They need to identify the most weakened towers and rank them in terms of criticality. Then, they will be able to plan investments and start maintenance actions.

Unfortunately, the life expectancy of such towers is not a standard feature since it depends on the mechanical load that was applied to the structure along its life cycle. The manufacturer generally estimates roughly the tower life expectancy according to the predictive use of the structure, but this initial estimation is actually never updated later.

The present report describes a research work about a non-destructive technique based on modal shape analysis whose purpose is assessing metallic tower masts condition at a given time.

On the one hand, vibrations are recorded on healthy towers to begin building a testing database and check the coherence with theoretical models. On the other hand, several boundary configurations are carried out to simulate structural defects and investigate the possible consequences of a local structural flaw on the whole structure modes of vibration.

> *Note: If the test protocol consists in measuring the vibrations in the mast of the tower, the objective is not studying the impact of vibrations in the structure. The measurement of vibrations is only a way to extract structural information from the tower.*

1.3. Key objectives and specific targets

- **Design and implement accurate protocols to record vibrations on a tower with different sensors**
  - Define the location of the sensors, acquisition parameters and excitation method for each testing
  - Develop tools to make the testing devices easy to install
- **Extract modal information of a structure from raw vibration measurements**
  - Differentiate natural vibration modes from other eventual frequency peaks.
  - Identify noise disturbances on signal and make assumptions about their origin.
  - Analyze the effects on mode shapes of an intentional damage to the boundary conditions.
- **Compare measurements to a theoretical model of the tower**

- Extract the tower geometry, build its 3D model and compute its theoretical modal shapes
- Confront theoretical model to operational measurements
  - Identify the similarity and differences for every configuration and try to explain them
  - Make suggestions to improve the numerical model regarding to experimental results on healthy structures

1.4. Scope of the investigation

The towers where experiments were performed are assumed to be in good condition.

It was only possible to induce reversible weaknesses that do not endanger safety of people or damage material.

The main objective of the present study was to identify the vibration modes from raw velocity recordings and to make assumptions about the phenomena that can appear on such results.

Only the tower mast vibrations were analyzed: no geotechnical study is provided. In particular, the soil-structure interaction is not part of this study and the case of a weakness inside the foundation is not investigated here. It remains possible to specify degrees of freedom in the numerical model between the ground and the mast and this way model the embedding condition.

No fatigue calculation was performed on the tower models. So, the remaining life expectancy of such tower has not been estimated.

Finally, this project research takes place within an internship framework. As a consequence, its duration is limited in time by an internship contract and cannot be extended beyond six months. Logistical constraints can delay the experiments achievement and postpone the data processing.

2. Theoretical background

2.1. Resonance phenomenon

Resonance describes the phenomenon of increased amplitude when applying a force at a frequency which is equal or close to a natural frequency of the system on which it acts. When an oscillating force is applied at a resonant frequency of a dynamic system, such system will oscillate at a higher amplitude than when the same force is applied at other, non-resonant frequencies. [5]

Such resonance phenomenon occurs for all types of waves or vibrations: mechanical resonance, acoustic resonance, electromagnetic resonance, nuclear magnetic resonance (NMR), electron spin resonance (ESR) and resonance of quantum wave functions.

ω_r is the resonant frequency of the system: $\omega_r = \omega_0\sqrt{1-2\,\zeta^2}$.

Such resonant frequency does not equal the undamped angular frequency ω_0 of the oscillator unless $\zeta = 0$.

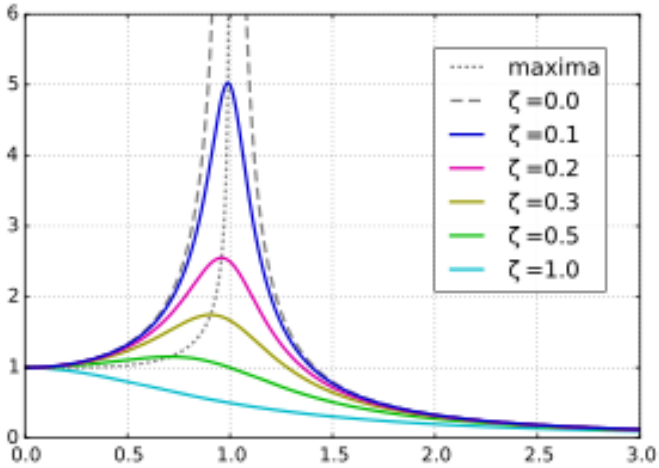


Fig. 1: Steady-state variation of amplitude with relative frequency $\frac{\omega}{\omega_0}$ and damping ζ of a driven simple harmonic oscillator.[6]

2.2. Analytic dynamic approach

A mechanical system has as many natural frequencies, and thus as many mode shapes, as Degrees of Freedom (DOF). Such modes are function of intrinsic and acquired parameters.

This point can be illustrated with the example of a 2 DOF spring-mass system including shock absorbers.

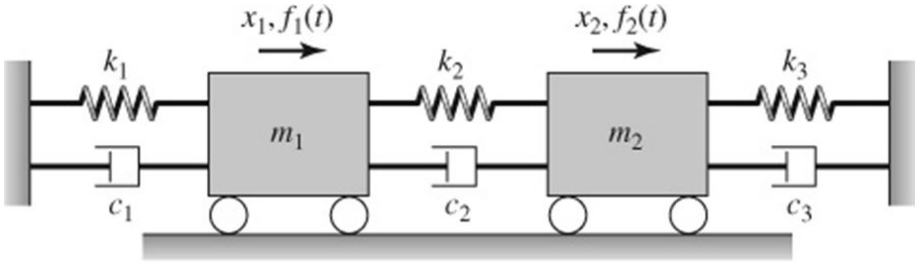


Figure 2: Diagram of a 2 DOF spring-mass system

Different types of forces can be identified:

- External forces $f_i(t)$
- Dynamic force proportional to acceleration
- Reaction F_k proportional to spring extension
- Damping force proportional to viscosity and thus to velocity

The expression of natural modes of vibration of a structure is a conservative phenomenon: all the mechanical energy implied is converted into a displacement. Thus, the general dynamic theorem in such context is valid:

$$M\ddot{u} = \sum F$$

- M the mass matrix
- ü the acceleration matrix (u the displacement)
- F the matrix of external loads

The equivalent formula for torque is:

$$I\ddot{\theta} = \sum Torques$$

- I the rotational inertia matrix
- $\ddot{\theta}$ the angular acceleration

In particular, the static balance equation can be written as:

$$[M]\{\ddot{u}\} + [C]\{\dot{u}\} + [K]\{u\} = \{f(t)\} \quad (1)$$

- M the mass matrix
- C the damping matrix
- K the stiffness matrix

When writing the static balance at the location of each mass of the 2DOF system described above, it is possible to set two equations:

$$\begin{cases} m_1\ddot{u_1} = -k_1(u_1 - 0) - k_2(u_1 - u_2) - c_1(\dot{u_1} - 0) - c_2(\dot{u_1} - \dot{u_2}) + F_1(t) \\ m_2\ddot{u_2} = -k_2(u_2 - u_1) - k_3(u_2 - 0) - c_2(\dot{u_2} - \dot{u_1}) - c_3(\ddot{u_2} - 0) + F_2(t) \end{cases}$$

The matrix representation of such model is:

$$\begin{bmatrix} m_1 & 0 \\ 0 & m_2 \end{bmatrix}\begin{Bmatrix} \ddot{u_1} \\ \ddot{u_2} \end{Bmatrix} + \begin{bmatrix} c_1 + c_2 & -c_2 \\ -c_2 & c_2 + c_3 \end{bmatrix}\begin{Bmatrix} \dot{u_1} \\ \dot{u_2} \end{Bmatrix} + \begin{bmatrix} k_1 + k_2 & -k_2 \\ -k_2 & k_2 + k_3 \end{bmatrix}\begin{Bmatrix} u_1 \\ u_2 \end{Bmatrix} = \begin{Bmatrix} F_1(t) \\ F_2(t) \end{Bmatrix} \quad (2)$$

2.3. Lagrange equations approach

Another way to come up with such matrixial system is writing the equations of Lagrange that deal with energy conservation.

Four types of energy can be involved in a mechanical system:

- Kinetic energy $E_k = \frac{1}{2}\sum m_i \dot{x}_i + \frac{1}{2}\sum I_i \dot{\theta}_i$
- Deformation energy $E_d = \frac{1}{2}\sum k_i (\Delta k)^2$
- Dissipation (Rayleigh function) $R = \frac{1}{2}\sum c_i \left(\frac{d}{dt}(\Delta c)^2\right)$

With Q_i the external mechanical actions, including generalized forces, the Lagrange can be written as:

$$\frac{d}{dt}\left(\frac{\partial E_k}{\partial u_i}\right) - \frac{\partial E_k}{\partial u_i} + \frac{\partial E_d}{\partial u_i} + \frac{\partial R}{\partial u_i} = Q_i$$

The generalization to N degrees of freedom leads to the same expression as for forces balance:

$$[M]\{\ddot{u}\} + [C]\{\dot{u}\} + [K]\{u\} = \{f(t)\}$$

2.4. Analytic resolution

2.4.1. Periodic signal assumption

The natural mode shapes only occur for given frequencies: it deals with the structure response to external periodic excitation. Thus, u(t) and f(t) can be written as follows, in every location x_i:

$$\begin{cases} u(x_i,t) = u(x_i)e^{-j\omega t} \\ f(x_i,t) = f(x_i)e^{-j\omega t} \end{cases}$$

The dynamic general equation $M\ddot{U}(t) + C\dot{U}(t) + kU(t) = F(t)$ becomes:

$$\begin{cases} -M\omega^2 U e^{-j\omega t} + jC\omega U e^{-j\omega t} + KU e^{-j\omega t} = F e^{-j\omega t} \\ (-M\omega^2 + jC\omega + K)\cdot U = F \quad \textit{(3)} \end{cases}$$

The natural frequencies are the eigen values of such system and the deformed shape its eigen vectors. This eigen value problem can be expressed as:

If there are no external forces applied, it is equivalent to:

$$(K + jC\omega - {\omega_i}^2 M)\phi_i = 0 \qquad (4)$$

- K the stiffness matrix
- C the damping matrix of the structure
- M the mass matrix of the structure
- ω_i the natural pulse of mode i
- ϕ_i the eigen vector of mode i, which is also the normalized deformed shape

2.4.2. Calculation of natural frequencies (eigen values)

The natural frequency is the frequency for which losses are minimal. It is possible to simplify the calculation of natural frequency by neglecting the damping effect. As a matter of fact, the damping ratio can influence the *resonance* frequency but not the *natural* frequency of the oscillator. [6]

By posing for instance $m_1 = 3m$, $m_2 = m$ and $k_1 = k_2 = k_3 = k$ the system is converted into:

$$\begin{bmatrix} 3m & 0 \\ 0 & m \end{bmatrix} \begin{Bmatrix} \ddot{u_1} \\ \ddot{u_2} \end{Bmatrix} + \begin{bmatrix} 2k & -k \\ -k & 2k \end{bmatrix} \begin{Bmatrix} u_1 \\ u_2 \end{Bmatrix} = \begin{Bmatrix} 0 \\ 0 \end{Bmatrix}$$

Solutions are harmonic and can be written as $u(t) = Ue^{rt} = Ue^{-j\omega t}$

$$\begin{bmatrix} 3mr^2 + 2k & -k \\ -k & mr^2 + 2k \end{bmatrix} \begin{Bmatrix} U_1 \\ U_2 \end{Bmatrix} e^{rt} = \begin{Bmatrix} 0 \\ 0 \end{Bmatrix} \qquad (5)$$

By calculating the determinant $(3mr^2 + 2k) \cdot (mr^2 + 2k) - k^2 = 0$, two non-trivial solutions can be identified:

$$\begin{cases} {r_1}^2 = -0.451\frac{k}{m} & \text{so} \quad r_1 = \pm j \cdot 0.672\sqrt{\frac{k}{m}} \qquad (6.1) \\ {r_2}^2 = -2.22\frac{k}{m} & \text{so} \quad r_2 = \pm j \cdot 1.49\sqrt{\frac{k}{m}} \qquad (6.2) \end{cases}$$

Since $r_i = \pm j\omega_i = \pm j \cdot 2\pi f_i$, the natural frequencies of such system are:

$$\begin{cases} f_1 = \dfrac{0.672}{2\pi}\sqrt{\dfrac{k}{m}} \\ f_2 = \dfrac{1.49}{2\pi}\sqrt{\dfrac{k}{m}} \end{cases}$$

2.4.3. Calculation of mode shapes (eigen vectors)

The deformed shapes $\begin{Bmatrix} U_1 \\ U_2 \end{Bmatrix}$ related to such natural frequencies can also be calculated for the not damped system by replacing the values of ${r_i}^2$ ***(6)*** inside the matrix system ***(5).***

For the first mode shape:

$$\begin{bmatrix} -0.451 \cdot 3k + 2k & -k \\ -k & -0.1451 \cdot k + 2k \end{bmatrix} \begin{Bmatrix} U_1 \\ U_2 \end{Bmatrix} e^{rt} = \begin{Bmatrix} 0 \\ 0 \end{Bmatrix}$$

$$\begin{cases} (-0.451 \cdot 3k + 2k) \cdot U_1 - k \cdot U_2 = 0 \\ -k \cdot U_1 + (-0.451 \cdot k + 2k) \cdot U_2 = 0 \end{cases}$$

Such displacements are expressed in terms of relative displacement from one point to another:

$U_2 = 0.646 \cdot U_1$ $\qquad \phi_1 = \begin{Bmatrix} U_1 \\ U_2 \end{Bmatrix} = \begin{Bmatrix} 1 \\ 0.646 \end{Bmatrix}$ ***(7)*** considering arbitrarily $U_1 = 1$

For the second mode shape, the same way:

$$\begin{bmatrix} -2.22 \cdot 3k + 2k & -k \\ -k & -2.22k + 2k \end{bmatrix} \begin{Bmatrix} U_1 \\ U_2 \end{Bmatrix} e^{rt} = \begin{Bmatrix} 0 \\ 0 \end{Bmatrix}$$

$U_2 = -4.65 \cdot U_1$ $\qquad \phi_1 = \begin{Bmatrix} U_1 \\ U_2 \end{Bmatrix} = \begin{Bmatrix} 1 \\ 4.65 \end{Bmatrix}$ considering still $U_1 = 1$

Finally, $\phi = \begin{bmatrix} \phi_{11} & \phi_{21} \\ \phi_{12} & \phi_{22} \end{bmatrix} = \begin{bmatrix} 1 & 1 \\ 0.646 & -4.65 \end{bmatrix}$ ***(8)***

Since such modes are **normalized**, they are defined to within one multiplicative constant.

2.5. Generalization to N-DOF system

For applying such mathematical model to a whole complex structure, it is necessary to mesh such geometry into very small simple elements called finite elements.

Such elements can adapt their shape to fit the object profile. Nevertheless, their shape always must be very simple for the calculation to be efficient.

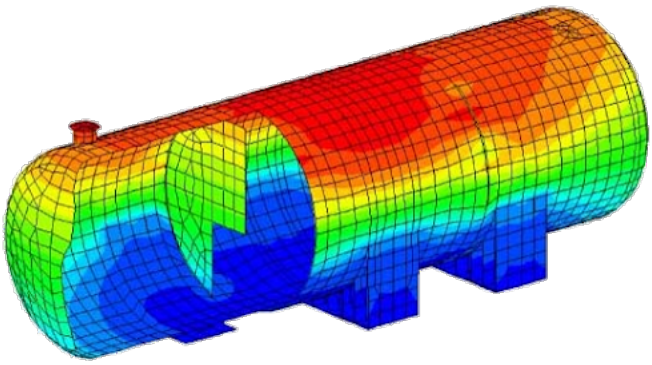


Figure 3: Meshing made of triangles and quadrilaterals, Source: http://www.blue-eng.fr/savoir-faire.html

The most common Finite elements are:

- Beam element - standard 2-noded element
- Plane elements – 3 node triangles (T3) and 4 node quadrilaterals (Q4)

Commercial software such as COMSOL, Robot Autodesk, ANSYS or SolidWorks, which performs mode shape analysis, all use Finite Elements Method. [21][22]

2.6. Theoretical Transfer Function

The *Transfer Function*, also known as *Frequency Response Function* (FRF), is a mathematical function which models the output of the structure for each possible input [24].

The FRF correlates the input excitation with the displacement of the structure in frequency domain and can be computed thanks to Fourier Transform algorithm. This FRF reveals which frequencies are amplified by the structure itself, regardless of the excitation spectrum.

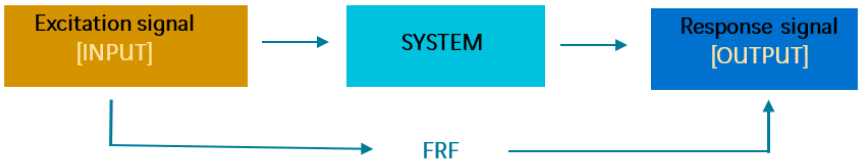


Figure 4: Vibration transmission process

Each resonance peak of the *Frequency Response Function* provides evidence of a natural vibration mode through magnitude and phase variations in the frequency spectrum.

The *Transfer Function* H(ω) of such system is the output displacement divided by the input force. From ***(3)***, it comes:

$$H(\omega) = \frac{F}{U} = [-\omega^2 M + j\omega C + K]^{-1}$$

By posing $c_1 = c_2 = c_3 = c$:

$$H(\omega) = \begin{bmatrix} -\omega^2 m + 2j\omega c + 2k & -j\omega c - k \\ -j\omega c - k & -\omega^2 \cdot 3m + 2j\omega c + 2k \end{bmatrix}^{-1} = \begin{bmatrix} \frac{U_1}{F_1} & \frac{U_1}{F_2} \\ \frac{U_2}{F_1} & \frac{U_2}{F_2} \end{bmatrix}$$

The transfer function for m=1 [kg]; k=10 [daN/m]; c=0.1 [kg/s] is plotted below.

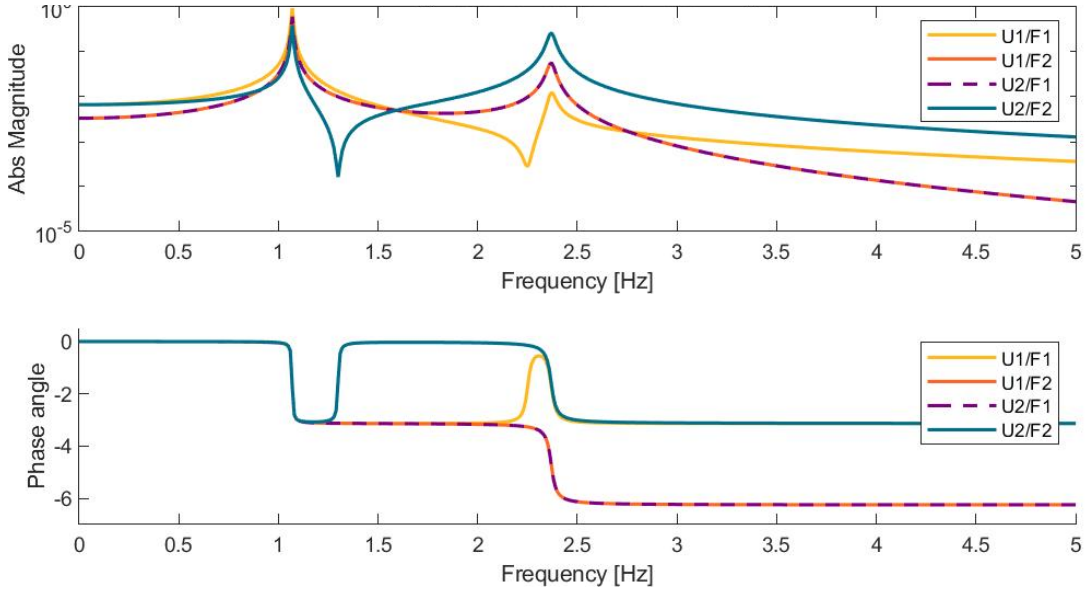


Figure 5: Transfer function of the 2-DOF-system

We can notice that $\frac{U_1}{F_2} = \frac{U_2}{F_1}$: the motion of the point 2 due a force applied at point 1 is exactly equal to the motion of the point 1 due to a force applied at point 2. This is the reciprocity principle.

Such transfer function shows two frequency peaks (1.07Hz and 2.37Hz) that corresponds to the resonance. The functions $\frac{U_1}{F_1}$ and $\frac{U_2}{F_2}$ contains each one an antiresonance peak (1.3Hz and 2.25Hz). Antiresonance is due to destructive interferences of both coupled bodies.

The eigen vectors of the system, which are actually the deformed shapes, can directly be extracted from the imaginary spectrum. Such imaginary part is due to damping force reactions to the resonance. The imaginary spectrum in the case of an external force applied to the mass m_2 is displayed below.

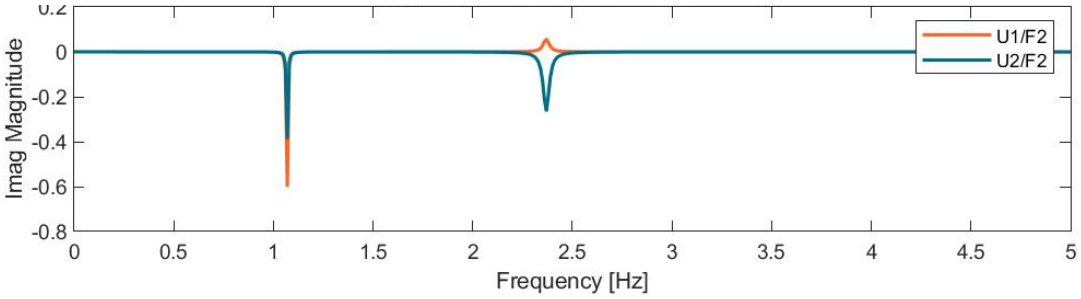


Figure 6: Imaginary part of the 2-DOF-system Transfer Function

The following values can be read on the graph:

$$Im(H_1(f_1)) = -0.601 \qquad Im(H_2(f_1)) = -0.388$$

$$Im(H_1(f_2)) = 0.0570 \qquad Im(H_2(f_2)) = -0.265$$

Such magnitude values do not have a significant meaning: only the relation between them must be analyzed. If we consider the same normative as for equation *(7)*, $U_1 = 1$, the eigen vector are exactly same as calculated in *(8)*:

$$\phi = \begin{bmatrix} \phi_{11} & \phi_{21} \\ \phi_{12} & \phi_{22} \end{bmatrix} = \begin{bmatrix} 1 & 1 \\ \frac{Im(H_2(f_1))}{Im(H_1(f_1))} & \frac{Im(H_1(f_2))}{Im(H_2(f_2))} \end{bmatrix} = \begin{bmatrix} 1 & 1 \\ \frac{-0.388}{-0.601} & \frac{-0.265}{0.0570} \end{bmatrix} = \begin{bmatrix} 1 & 1 \\ 0.646 & -4.65 \end{bmatrix}$$

Since the transfer function do not depend on the external excitation, the same calculation for a force applied in the mass m_1 lead to the same eigen vector: $\phi = \begin{bmatrix} 1 & 1 \\ \frac{-0.601}{-0.931} & \frac{0.0570}{-0.0123} \end{bmatrix} = \begin{bmatrix} 1 & 1 \\ 0.646 & -4.63 \end{bmatrix}$.

2.7. Experimental approach

2.7.1. Fourier Transform

Fourier analysis converts a signal from its original time (or space) domain to a representation in the frequency domain and vice versa. The *Discrete Fourier Transform* (DFT) is obtained by decomposing a sequence of values into components of different frequencies. [2] The DFT which represent the transformation $x_n \rightarrow X_k$ is obtained by the following formula:

$$X_k = \sum_{n=0}^{N-1} x_n e^{-j2\pi kn/N} \quad \forall k = 0, \dots, N-1$$ where $e^{-j2\pi kn/N}$ is a primitive N[th] root of 1.

X_k can be expressed as an inner product:

$$X_k = \begin{bmatrix} 1 & e^{-j2\pi kn/N} & e^{-2\cdot j2\pi kn/N} & \dots & e^{-(N-1)j2\pi n/N} \end{bmatrix} \begin{bmatrix} x_0 \\ x_1 \\ \vdots \\ x_{N-1} \end{bmatrix}$$

The *Inverse Discrete Fourier Transform* (IDFT) that represents the transformation $x_n \rightarrow X_k$ is obtained by the following formula:

$$x_n = \frac{1}{N} \sum_{k=0}^{N-1} X_k e^{j2\pi kn/N} \quad \forall n = 0, \dots, N-1$$

$$x_n = \frac{1}{N} \begin{bmatrix} 1 & e^{j2\pi k/N} & e^{2\cdot j2\pi kn/N} & \dots & e^{(N-1)j2\pi kn/N} \end{bmatrix} \begin{bmatrix} x_0 \\ x_1 \\ \vdots \\ x_{N-1} \end{bmatrix}$$

A Fast Fourier Transform (FFT) is an algorithm that computes the discrete Fourier transform (DFT) of a sequence. It rapidly computes such transformations by factorizing the DFT matrix into a product of sparse (mostly zero) factors.[3]

When performing a measurement, the acquisition is made for discrete instants of time which duration depends on the sampling frequency. The Fast Fourier Transform is an indispensable tool for identifying periodicities in the raw signal.

2.7.2. Response of the system

The transfer function, or *Frequency Response Function* (FRF), is intrinsic to the structure, placed in given boundary conditions: it is a sort of signature of such structure. However, the transfer function is not measurable directly by fixing sensors on a structure since the response of the structure actually depends also of the input excitation.

When the excitation measurements and the structure displacement measurements are synchronized, it is possible to establish the FRF at each measuring point since $H(f) = \frac{U(f)}{F(f)}$.

Rigorously, the transfer function is generally estimated with the H_1 Welch estimator in commercial software such as Matlab [18]:

$$H_1(f) = \frac{F(f) \cdot U(f)}{F(f) \cdot F(f)} = \frac{Cross\ Spectral\ density\ of\ the\ Input\ and\ Output}{Auto\ spectral\ density\ of\ the\ Input}$$

As an example, the following graph has been drawn for the data of the previous 2DOF system. The three curves represent a simulation of the system response to different types of excitation. Such plots were performed on Matlab software by using the relation $U(\omega) = \frac{F(\omega)}{H(\omega)}$.

The different types of input excitation signals that were tested in the program are plotted below in frequency domain for an 8 minutes signal with a 128Hz sampling frequency.

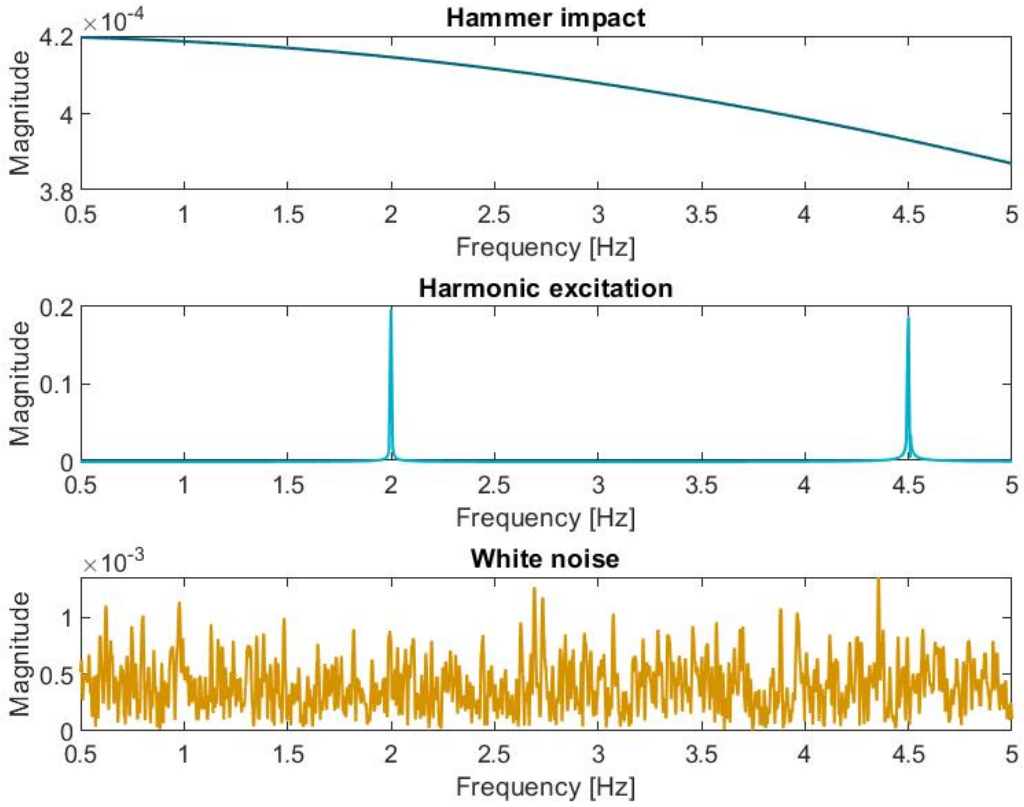


Figure 7: Simulation of the Frequency spectra of the different types of input excitation, Fs = 100Hz

We can see that the frequency distribution is not neutral at all for the periodical excitation. Regarding to broadband excitation methods, the frequency composition of the signals is not necesarily a constant either. Though, statistically, the longer the recording, the more the frequency distribution of the excitation is close to a constant.

When release energy to the 2-DOF-system with this different types of excitation, we obtain the following response:

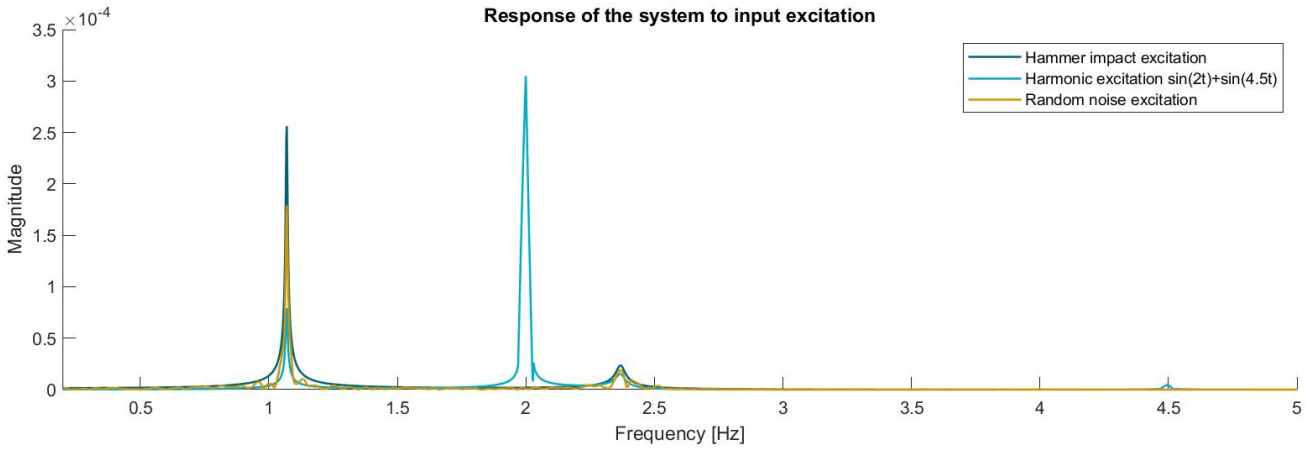


Figure 8: Simulation of the Response curve shape depending on the type of input excitation, Fs = 100Hz

For broadband excitation methods such as impact or random noise, the response frequency spectrum seems to draw two clear peaks for the natural frequencies 1.07Hz and 2.37Hz.

For a harmonic excitation, the response spectrum contains not only the peaks at the system natural frequency, related to the structure resonance, but also other peaks related to the excitation signal (2Hz and 4.5Hz). Besides, despite the system receives the same energy at 2Hz and 4.5Hz, the peaks corresponding to such frequencies appear with different magnitudes in the response spectrum.

As a matter of fact, if the input harmonic signal is close to a natural frequency of the system, it will make it vibrates with an important magnitude. [53]

As a consequence, it is very important to correlate the system response to the input excitation to extract the transfer function from measurements. So, the input excitation has to be, or controlled, of measurable.

Yet, in the case of a hammer impact or an ambient noise testing, the absolute magnitude of the Response can provide a reliable estimation of the natural frequencies and related mode shapes. The imaginary and real part, however, do not always contain relevant information.

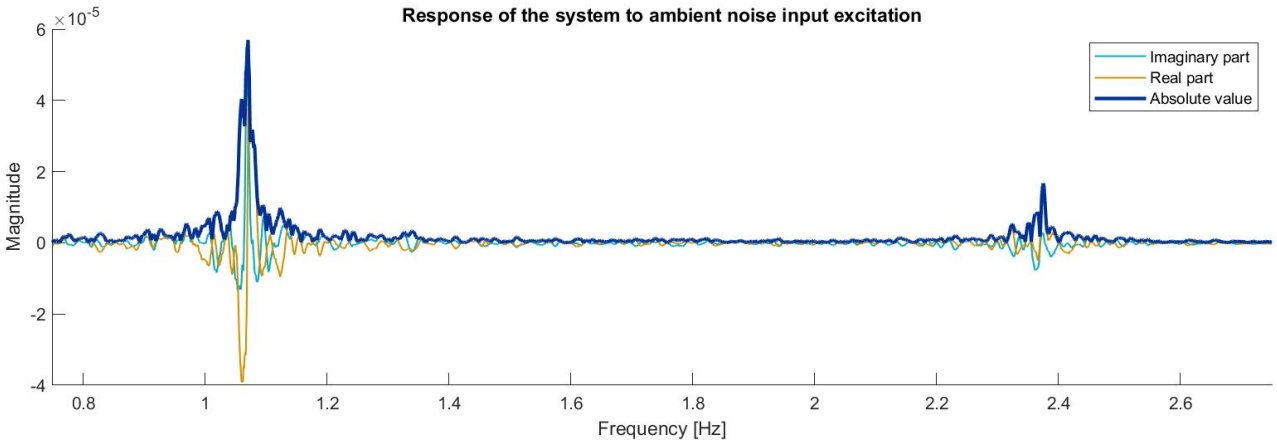


Figure 9: Response of the 2-DOF-system to ambient noise vibrations

As a conclusion, for a given structure, the same frequency peaks - although with different scales because natural excitation is not exactly random, should appear both in the response and in the FRF when looking at the magnitude spectrum.

So, it is possible to identify natural modes of a structure by measuring only the structure velocity. Though, if the input excitation is not controlled, the frequencies may be subject to error. In particular, by considering only the output signal instead of the FRF, it is difficult to prove substantially the existence of the vibration modes:

- The presence of frequency peaks can be influence by input excitation
- Imaginary and real part of the spectrum do not contain information.
- Phase angle do not register a sudden change like in FRF: only the relative phase difference between the sensors can be useful to determine the direction of relative movements.

3. Literature review

Plenty of technologies for Non-Destructive Testing (NDT) are used for heavy industry, especially for oil, naval, aircraft, aerospace, military, and automotive industries. In general, such inspections are conducted in laboratories since the tested parts are not assembled yet. It is quite common to combine several NDT to get a complete overview of the flaws. [28][31]

However, engineering structure are usually huge and located outside, not all these technologies are possible to carry out.

3.1. Visual inspection

The towers are all equipped with at least one ladder so that authorized personnel can inspect it. Despite this audit is relatively quick to carry out, it is not exhaustive.

Not every surface is always accessible from the ladder and some flaws can be hidden by the painting or by the structure itself. For instance, most of swiss power-line towers are made of old pipes that are filled with concrete. So, corrosion is more likely to occur inside than outside the pipes.



Figure 10: Corroded tubular frame filled with concrete

3.2. Dye penetrant inspection (DP)

Dye penetrant inspection (DP), also called liquid penetrate inspection (LPI) or penetrant testing (PT), is used to highlight surface-breaking defects in all non-porous materials such as metals, plastics, or

ceramics. Basically, its principle is spreading a penetrant fluid on the surface of an object and identify failures with a developer. [30] This process is made across the following steps:

- Pre-cleaning
- Application of penetrant
- Excess penetrant removal
- Application of developer
- Inspection
- Post cleaning

Thanks to DP, it is possible to detect casting, forging, and welding surface defects such as hairline cracks, surface porosity, leaks in new products, and fatigue cracks. [29] It is widely used in many types of industry because low cost. However, for a huge structure like a metallic tower, it can imply a very long process.

3.3. Ultrasonic Testing (UT)

Ultrasonic inspection is a method that uses the sound wave reflective property while changing its propagation medium. In most of the applications, very short ultrasonic pulse-waves are transmitted into materials in order to detect internal flaws or to characterize materials. This technology is often used to measure the thickness of the test object, for example, to monitor pipework corrosion. [27]

The device contains a transmitter-receiver probe. The probe is typically separated from the test object by a conducting gel (couplant). The wave comes perpendicular to the object surface and propagates through the material until its composition changes. Then, part of this wave is reflected and comes back to the probe. The device measures the time between wave emission and reception and deduce the material thickness from the velocity of sound in this medium.

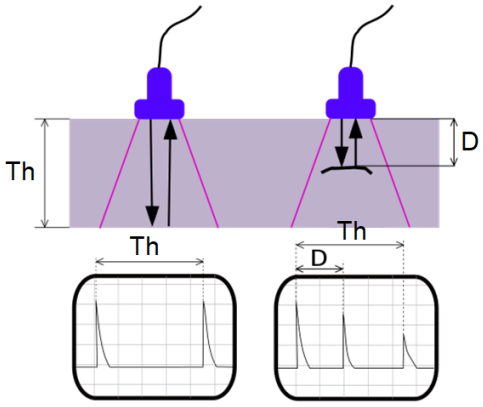


Figure 11: Principle of ultrasonic testing [25]

Ultrasonic testing is usually performed on metals and alloys. It can also be used for concrete, wood and composites, although with less resolution. [26]

Applying this technology to a huge structure to detect local section reductions for instance can seem quite arduous since it is a punctual method. However, the process can be automatized with robots. Some engineering companies such as *Mistras®* already offers such services for metallic structures inspection [35].



Figure 12: Ultrasonic large structure inspection device [35]

Ultrasonic Pulse Velocity (UPV) can also be used to evaluate the quality of concrete near to the pile head. By evaluating the average UPV in the concrete, it is possible to assess the general quality of concrete mix. Low strain pile integrity test



Figure 13: Ultrasonic Pulse Velocity measurements on a ski-lift tower [36]

3.4. Eddy Current Testing (ECT)

Eddy Current Testing makes use of electromagnetic induction to detect and characterize surface and sub-surface flaws in conductive materials.[32][33]

The device, schematized on the opposite figure, detects variations in the electrical conductivity and magnetic permeability of the test object.

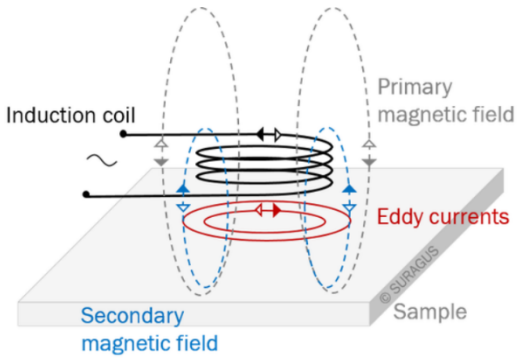


Figure 14: Eddy Current Testing principle [32]

Corrosion of a steel element is an electrochemical process. It acts as a galvanic cell in a similar way to a battery producing an electric current. This current can be measured on the surface as an electric field and compared with an electrode at a standard potential. [38]

The presence of defects can imply changes in eddy current phase and amplitude that can be detected when measuring the impedance variations in the coil.

This technique, although limited to conductive material, is very sensitive and can even detect tight cracks. Wall loss or corrosion can be detected but without confidence regarding to sizing. This alternative can be interesting in case of pipe inspection or when a conductive material is hidden behind an electrical insulator.

As for ultrasound testing, the detection of local flaws with an Eddy Current device requires automatization, the use of a robot for example, to be applied to large structures. [34]

However, it is an interesting tool for detecting corrosion issues on the embedding. As a matter of fact, it is common that the anchor rods of the tower react with the concrete slab and get weakened. A current ΔI is applied while recording the change in electric potential ΔE that occurs between the half-cell and the corroding sample.

JF Strainstall company performs this type of NDT. The electrode spike is driven into the ground within 1m of the component, to a depth of at least 200mm. The BGCMAP unit is connected to the component and the electrode using heavy duty steel clips. The test is carried out automatically by the device, which applies a current and records the voltage. [38]



Figure 15: Eddy current device by JF Strainstall called BGCMAP unit [38]



Figure 16: Example of corrosion of rods

3.5. Modal analysis

Nowadays, modal analysis for metallic towers is still experimental. The main focuses of the existing studies are improving the reliability of Finite Element models.

It is possible to measure vibrations of a huge structure with accurate sensors. Signal processing tools can highlight its bending and torsion modes of vibration and related deformed shapes. Then, it is possible to compare theoretical modes of vibration to operational ones: structural analysis software can simulate the vibrating behavior of a structure since its geometry and composition are known. A tower can be assimilated to a beam for example.

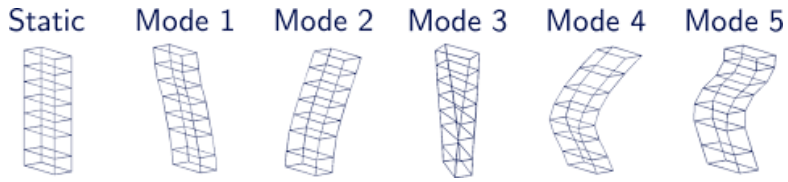


Figure 17: First theoretical mode shapes of a beam

If a vibratory campaign has been performed when installing the line, it is also possible to assess a structural change by following the evolution of modal parameters.

It exists a large variety of sensors able to record such low frequency vibrations. Accelerometers, velocimeters, displacement sensors. [45]

Lastly, a MIT study [46] brought to light a movement amplification method. A camera records a high-quality video of the structure that is computed to a powerful image processing software. Every pixel movement can be then amplified, and the video can be filtered at a specified frequency.

3.5.1. Conventional modal analysis

Accelerometers are often used for conventional laboratory modal testing. A controlled excitation is applied to the test object and its vibratory response is recorded by sensors. This input force can be provided by a modal hammer or a vibrating table for instance. [2.7] Thanks to reciprocity principle, the transfer function can be obtained by using one and only sensor and shock the structure in successive locations or by arranging sensors all around the structure and excite it in a single location.

Controlling the excitation of a whole tower can be very complicated since it requires a lot of energy. Though, it is possible to build a scale model of the structure for carrying out testing on it. Er. Chiranjit [39**Erreur ! Source du renvoi introuvable.**] led such a project on a transmission tower and compared the results to numerical models build on ANSYS and STAAD Pro.

Note: The objective was not to assess the condition of the structure in this study. However, building a scale model might be an interesting tool to simulate defects on a structure.

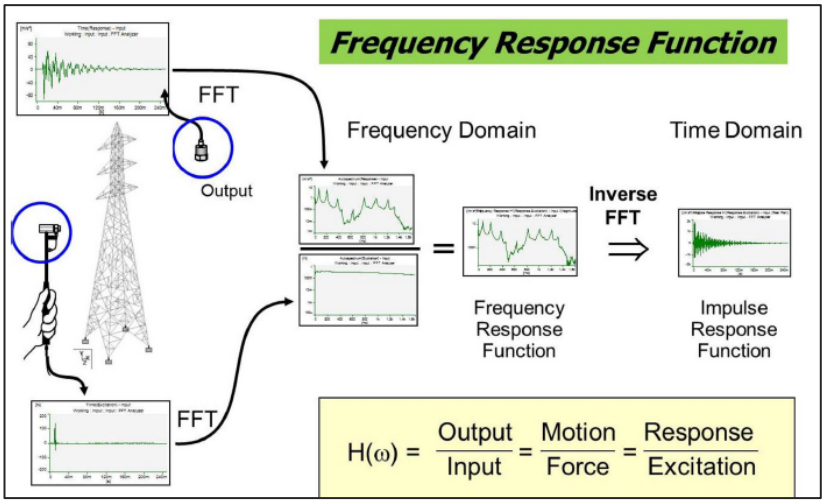


Figure 19: Principle of the measurement and signal processing

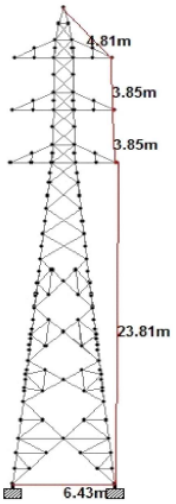


Figure 18: Dimensions of the scale model

Such model was build with a scale factor of (1:15), so the measured frequencies have to be divided by 15 to estimate the real tower natural frequencies. The same mode shapes was identified for the modelling and the numerical model, with frequency actually very close to each other (standard deviation 5%).

Mode	Frequencies obtain from ANSYS (Hz)	Frequencies obtain from STAAD Pro.(Hz)	Natural frequencies of scale-down model (Hz)
1	2.1773	2.1045	30.6595/15 = 2.043
2	2.1870	2.887	30.2506/15 = 2.016
3	5.3096	3.546	81.2617/15 = 5.417
4	6.9248	6.953	101.0672/15 = 6.737
5	7.0498	7.252	118.9234/15 = 7.928
6	7.3412	8.793	126.1435/15 = 8.409

Figure 20: Theoretical and modelled natural frequencies

Another application of conentional modal analysis on towers is the Pile Integrity Test (PIT), or "low strain impact integrity testing of deep foundation". This is a widely used non-destructive test method for the evaluation of pile quality, and integrity. In the low strain impact integrity testing, the response of the pile to a hammer impact on the head of the pile shaft is determined by a high precision transducer mounted on the pile head. The transducer can either be an accelerator, or a velocity sensor. [40]



Figure 21: Example of a portable unit which performs the acquisition of acceleration measurements [40]

Such test can also be conducted to estimate the unknown length of existing piles and foundations.

3.5.2. Natural excitation mode shape analysis

It is not always convenient to provide an external excitation to a structure, especially since the natural vibrations of the environment already provides a wide range of frequencies allowing the civil engineering structures to enter in resonance. The structures are vibrating naturally all the time and express this way their natural mode shapes. [47][48]

It is possible to measure the structure instantaneous response from natural vibrations with sensors, but the Frequency Response Function would be hard to compute. As a matter of fact, the input excitation is provided by many different sources (wind, seismic activity, cables, etc.) in many different locations of the structure.

Yet, these natural vibrations could be considered as random enough to behave as white noise [47][48], that is to say, it includes all the frequencies. Therefore, it is technically possible to extract the natural frequencies and associated mode shapes directly from the output signal. If the device sensitivity is limited, it remains possible to apply shocks to the structure since shocks are also involving a very large range of frequency (like a Dirac).

The scientific community registers investigations in different types of mast using this technology: buildings, metallic towers, rocket launcher, etc. Most of such studies are focused on the comparison between a real tower and its numerical model.

Such acquisition with random excitation is possible with accelerometers, velocimeters or displacement sensors such as optical fiber. The optical fiber may be the most precise equipment because providing a continuous recording all along the structure.

Still, discrete measurements with accelerometers are normally preferred for being cheaper, especially with the emergent MEMS technology: very small accelerometers like the smartphones one. Velocity sensors are quite more expensive than accelerometers since they are less noisy at low frequency [43]. They appear as an interesting compromise between precision and financial aspects.

Accelerometers are mostly utilized when the vibration level is strong enough. A paper from *Rome university* [51] shows a comparison between conventional modal analysis (with controlled excitation) and natural excitation modal analysis, both performed with accelerometers. The scientist performed testing on a 30 meters high launcher. Both analyses lead to similar results: same frequencies and deformed shapes.

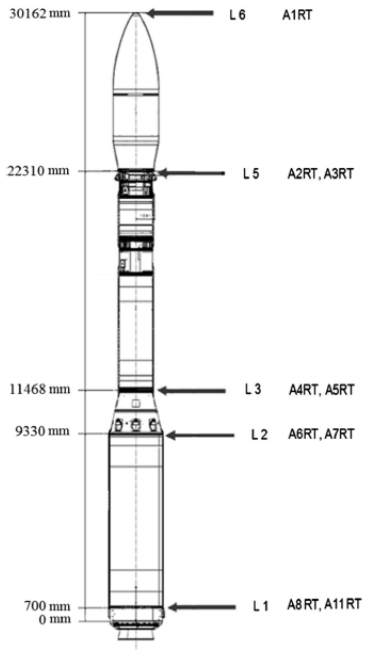


Figure 22: Layout of the accelerometers for experiments on the launcher

The company Kinetrics performs modal analysis in ambient noise on powerline towers, using accelerometers (measurements of the local movement of the tower) and strain gauges (measurements proportional with the forces in the tower components). Their project monitors the One Nevada Line towers to ensure wind-induced vibration do not cause operational issues with the transmission line. The purpose here is to assess the vibration stresses and loading on a structure due to wind. This data can be used effectively to support confidence in the safety and reliability of the powerline.

A similar investigation was performed on a powerline tower in the margin of Guamá River and presented at the 13th International Congress on Sound and Vibration. With only six low frequencies accelerometers, the experimental and Finite Elements modal parameters were in very good agreement for the first three modes. For higher frequency, the results do not match and, according to the authors

of the study, it probably means that the FE model could not represent precisely the behavior of the structure at higher frequencies. [44]

Still, most of the projects of modal analysis were carried out on buildings, among them, the thesis of F. Dunand for *Bureau Veritas* [47]. He performed modal shape analysis with accelerometers under ambient vibrations. He studied the correlation between earthquake damages on buildings and changes in their modal parameters. In particular, the frequency of vibration modes goes down after a damage (up to 40%), so does damping: the rigidity of such buildings must be affected. However, F. Dunand warns about the probable non-linearity of such frequency drop because the recorded frequency can vary along the amplitude of solicitation. This technique can possibly help to assess the health status of a building, and also can be used to check repairs efficiency on it.

In the *university Joseph Fourier*, a few publications also relate modal shape analysis under ambient vibrations applied to buildings.

The *Institut de Recherche pour le Développement* developed and patented, together with their research partners, the acquisition center *Cityshark II*. They currently work on velocity recordings from vibrations induced by seismic tremors. They are able to build the operational deflection shape of such building by disposing several velocity sensors along a tower. [52]

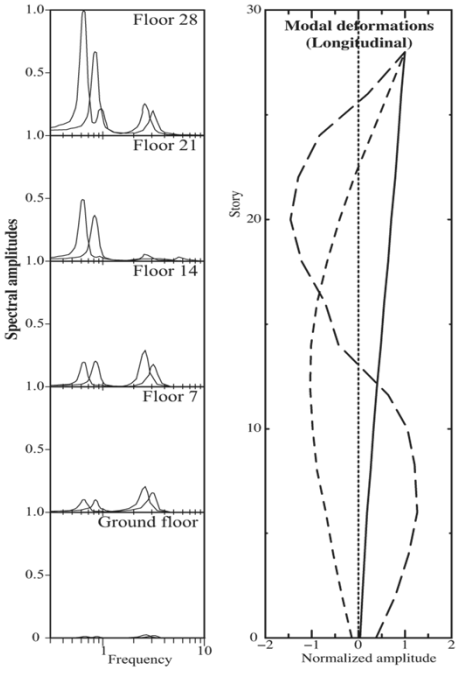


Figure 23: Building operational deflection shapes obtained thanks to Cityshark device

4. Methodology

The project consists in studying modal parameters on metallic towers and can be divided in three parts: experimental testing, signal-processing and structural theoretical analysis. After recording the vibrations in a tower mast, a post-treatment must highlight several modes of vibration, their natural frequency and their respective deformed shape. It is basically like taking a picture of the tower structure at a given moment of its life cycle. It is possible to compare then such experimental results to theoretical ones by building a 3D model of the tower in its exact dimensions.

Two campaigns where performed: one on a ski-lift tower, another one on a power-line tower. These towers were climbed by qualified staff.

4.1. Measurements

4.1.1. Type of sensors

Most of the trials were performed with velocimeters[19] in ambient noise. A velocimeter has a high sensitivity and works in a reduced range of amplitudes. So, it is convenient to use it in ambient noise. It consists in a magnet whose endpoints are hung by springs into a coil. When a wave comes to the tower, the coil follows its vibrations. Meanwhile, the magnet, thanks to its own mass and the spring inertia, gets its own vibrations which are much slower than those of the coil. This difference generates a magnetic field inside the coil and creates an alternating current.

The velocimeter devices used for such project also contained a 3D-MEMS accelerometer. MEMS bandwidth can go down to very low frequencies but the signal-to-noise ratio is extremely bad under 3Hz.

Some trials were performed with piezoelectric accelerometers[20] that can detect vibrations above a threshold a little higher. Therefore, it was convenient to hit the structure to get stronger vibrations.

Such tests were performed with uncontrolled shocks.

4.1.2. Acquisition parameters

A recording should last several minutes to get a good frequency resolution: $\Delta f = \frac{1}{duration}$. For the main part of recordings, a duration of 8 minutes was chosen. It provides a 0.002Hz resolution. It is more than necessary but it provides an overview of the variations of frequency spectrum across the time.

The sampling frequency should be at least twice higher than the highest mode frequency in order to compute data using Fast Fourier Transform. The first modes of such towers are included between 0 and 20Hz. Despite a 64Hz sampling frequency would be enough, it is convenient to choose Fs = 128Hz as a compromise between precision and calculation time.

For each measurement, it would have been relevant to perform twice the acquisition. This is a way to check whether the measure is reliable and to estimate the statistic error for given conditions. Unfortunately, time was missing for duplicating such measurements.

4.1.3. Sensors setting

The velocimeters were fastened to the mast with a metallic bracket and a strap. A spirit-level can help to install it horizontally. The bracket shape can adapt to any profile of tower and a large range of diameters. It was built tailor-made.[1]

It is not possible to fix velocimeters to the tower with a magnet without disturbing the measurements. Nevertheless, it is relevant to use a switchable magnet as an installation tool to free the climber hands while setting the strap.

If the company decides to finally buy such sensors and not only rent them, an easier fixation system will probably be developed to get closer to the structure.

An accelerometer, on the contrary, can be installed very quickly with magnets. A portable model generally weighs around 50g versus 500g for our velocimeters.

Climbing a tower requires security habilitations. These certifications are quite expensive and need to be renewed every year. Moreover, almost every country asks for a different certification. It is sometimes more cost-effective renting local climber services for a few days, especially when working abroad. But working with external operators requires organization to make instructions understandable. In particular, the operators must place the sensors at a certain place and in a certain direction. Therefore, it is important to mark every equipment with colors, letters, or arrows for instance. On the other hand, the project manager needs to control that every device is set at the right location, so the supports were also marked below.



Figure 24: Bracket marking

4.1.4. Sensor's location

The sensors were disposed, all along the same cartesian direction given by the structure symmetry: all along the mast and aligned on the top. The symmetrical axes of the tower are theoretically the modes shapes preferential directions.

The sensors on the top are useful to detect torsion modes but also transversal flexion modes through vertical velocity.

One of the sensors is located directly on the concrete to assess the embedding condition.

The weld seam of the tower mast can introduce variations of the mode shapes if it is weakened. So, if and only if the sensors are calibrated exactly the same way from one to another, it can be relevant to place a sensor at each side. It is not always easy to get such information from the provider.



Figure 25: Sensors fixed on a ski-lift tower with brackets

4.1.5. Ski-lift tower test campaigns

Two campaigns were performed on a same ski-lift tower:

- a campaign with 7 wireless 3D-axis velocimeters combined with MEMS 3D-axis accelerometers
- a campaign with 3 piezoelectric uniaxial wired accelerometers

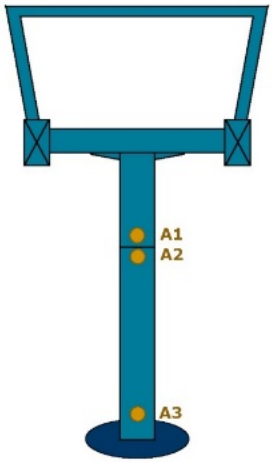


Figure 26: Piezoelectric accelerometers configuration on the ski-lift tower

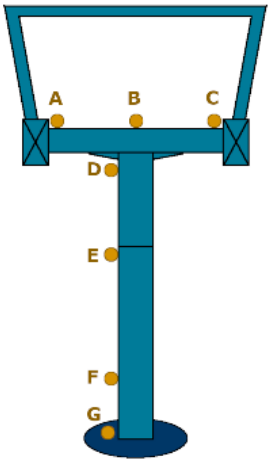


Figure 27: Velocimeters & MEMS configuration on the ski-lift tower

The reference configuration is a tower fixed with its eight bolts on the ground and without any load applied on his top.

Besides, other measurements were performed with different boundary conditions:

- Half of the bolts unscrewed to simulate a problem in a foundation



Figure 28: Connection of the ski-lift tower to the ground by bolts in a concrete slab

- Both side of the tower were loaded to simulate the cable tensed with nacelles. Tension values in this type of ski lift cables is around 15 o 20daN which represents approximately 2 or 3 tonnes in the vertical axis. Thus, the head of the tower was loaded as much as possible with a hand winch, here with 1.5 tonnes.



Figure 29: Direction of load for ski-lift cables in real conditions

Another trial was performed with only one side loaded with 1.5 tonnes. It aimed at studying the effect of inequal tension of the lines when one line goes up and the other goes down. One line is full of people while the other is empty, so one cable in tense while the other is released.

It would have been very complicated to reproduce exactly the operating loading conditions, so the load was applied in vertical axis only, which is the one that undergo almost all the load.

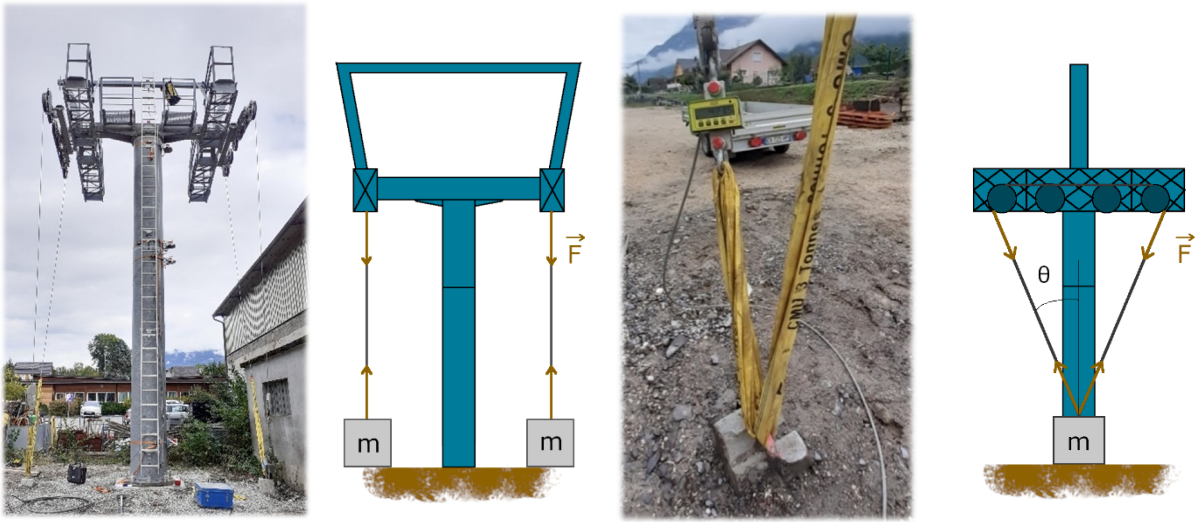


Figure 30: Experimental device to load the ski-lift tower on its two sides

4.1.6. Power-line tower test campaign

A test campaign was performed in Pont-du-Château high voltage training academy (CHTF)[3] on a G4S1R1 tower[4]. Thirty-five meters high, this is one of the French most common high voltage towers. Although it was a training academy, all the towers were placed under real conditions with cables tensed. The current was switched off.

Seven velocimeters were disposed along the tower but they were moved from one frame to another in order to record the whole structure vibrations. Two sensors (A & F) had a fix location because they acted as a reference for all the tests. This reference ensured whether or not all the frames were vibrating together at each frequency, in the same direction, and helped for normalizing amplitudes on the different acquisition. Therefore, it is possible to equip separately each frame and gather the measurements numerically. Each measurement lasted eight minutes.

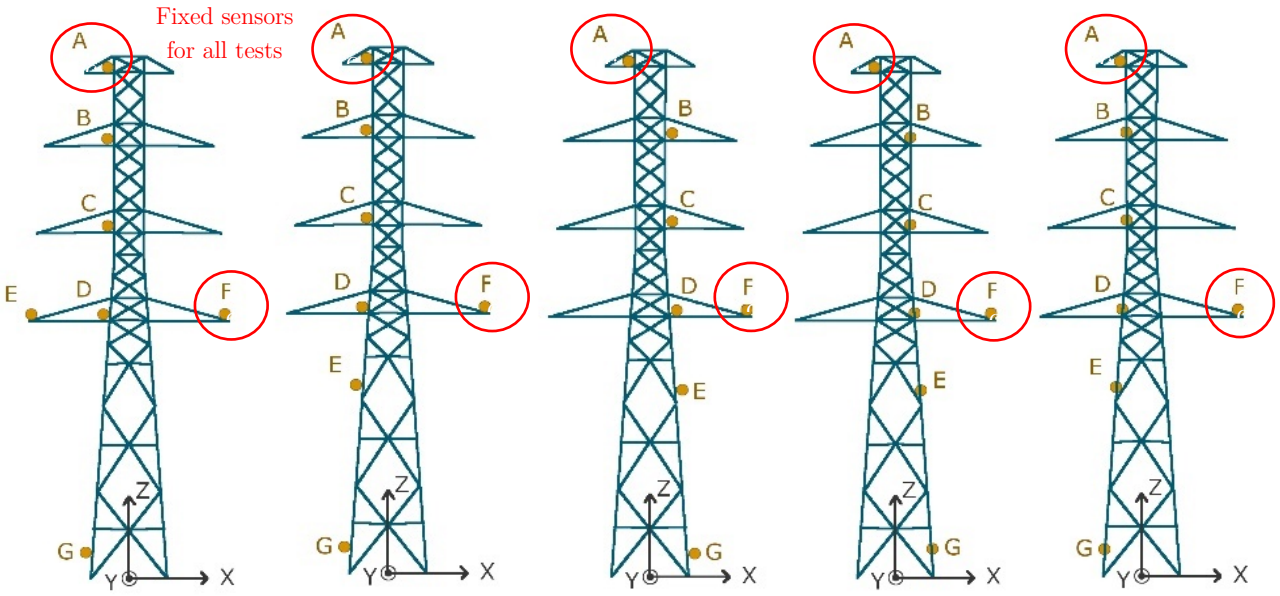


Figure 31: Sensors configurations for the testing on a power-line tower

Another test campaign aimed at assessing the transmission of vibration on the ground. he seven velocimeters were disposed in the following arrangement:

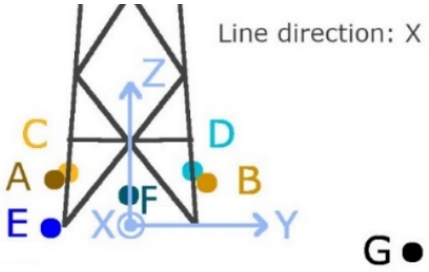


Figure 32: Sensors location on the powerline tower for studying soil-structure interaction

- A,B,C,D were fixed at the bottom of each frame
- E was placed on the ground just next to A frame
- F was placed on the ground at the center of all feet
- G was placed on the ground 15 meters away

The training academy also makes a high voltage cable installation available at ground level between two little beams. The current was switched off, but the cable was tensed like in real conditions and linked to the structure with isolators.

Quick tests were performed to understand the vibration behavior of such a cable.[5] A sensor was located on one of the beams and another one was fixed to the cable. Recordings were performed under ambient excitation and later while hitting slowly the cable with the hand.



Figure 33: Experimental device to record cables vibrations

4.3. Post-processing

When performing a modal shape analysis, three parameters are often extracted from raw measurements:

- The frequency of the modes of vibration
- The related Operational Deflection Shape, in other words the normalized biggest displacement of a structure at a given vibration mode
- The damping of each mode that represents how quickly such vibrations are dissipated.

In this study, the damping will not be analyzed since it is mainly defined by the material and not really by the structure geometry or the boundary conditions.

4.3.1. From time signal to frequency spectra

Natural frequencies and mode shapes are extracted from a Fast Fourier Transform (FFT) of the measured velocity. The frequency domain uses complex numbers, defined both by a magnitude and a phase angle. Basically, the FFT algorithm performs a frequency decomposition by checking the correlation between the raw signals and perfect sinusoids composed of only one frequency. The algorithm determines such coherence for a finite number of discreet frequencies between 0 and the Nyquist frequency $\frac{F_S}{2}$ Hz. When the two signals are correlated, the FFT has a high amplitude, so a peak appears on the spectrum. The more the time signal is long, the better is the frequency resolution of FFT spectrum $\Delta f = \frac{1}{recording\ duration}$.

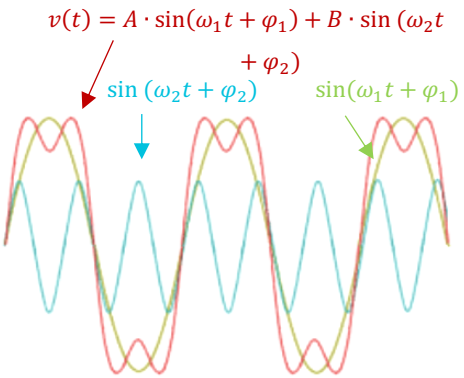


Figure 34: principle of FFT algorithm

A frequency peak in the FFT magnitude shows a high probability of a vibration mode: the structure is responding to the mechanical load by vibrating.

Since we have no way to measure the ambient vibrations the tower receives, we assume they are similar to white noise, at least in the frequency range [0;20] Hz. Thus, we suppose that, statistically, in the whole sample, all the frequencies are exciting the tower at the same amplitude. This way, the frequency peaks in the frequency response should correspond to the natural modes of vibration of the structure. [3.5.2]

In MATLAB software, the function *findpeaks* can help to automatize the peak research by specifying a magnitude threshold, a minimum peak prominence, the minimum distance between two peaks, etc.

4.3.2. Drawing deformed shapes

Despite the FFT magnitude is not expressed in scientific units, the relation of proportionality between all the sensors is correct. This way, the absolute value of relative displacement for all sensors can be directly extracted from the FFT.

Then, the FFT algorithm not only compute the magnitude of velocity displacement for each sensor but also the phase angle that indicates which sensors move together and which ones go in the opposite direction. In-phase devices for a given frequency will show a phase difference multiple of 2π whereas signals in phase opposition will show a $(2\pi+1)n$ phase difference. It is possible then to build the deformed shapes by defining the sensor that registers higher magnitude at such frequency as a reference for positive sign for instance.

Despite the deformed shape represents actually the biggest displacement of a structure at a given vibration mode, it is often expressed a normalized way: the highest displacement value is set to 1: the amplitude of such displacement is not as relevant as the proportionality between the displacement of all sensors.

Another way to express such displacement would be the complex writing:

$$U(t_N) = j\omega \cdot V(t_N)$$

As a consequence, at a given frequency, there is a linear relation between Velocity and displacement for all sensors. In other words, if U_N is the displacement vector for all sensor position and V_N the corresponding velocity vector, we can write, at a given frequency: $U_N = \alpha \cdot V_N$.

As a consequence, it is not necessary computing the integration of the signal to get the normalized operational deflection shapes for all modes of vibrations since it can be extracted directly from velocity raw signals.

Though, getting displacement from velocity would not be a complicated staff. We could easily calculate such instantaneous displacement $U(t_N)$ thanks to Riemann integral in time domain:

$U(t_N) = \sum_{i=1}^{N} V(t_i) \cdot \partial t_i = \Delta t \cdot \sum_{i=1}^{N} V(t_i)$ with $\Delta t = \frac{1}{F_s}$.

4.3.3. Visualize the deformed shape a dynamic way

It is also possible to filter the frequency signal to pick only one mode and draw back the time signal applying Inverse Fast Fourier Transform. The IFFT function returns a complex number since it represents a signal in the form of $v(t) = \sin(\omega t) + i\cos(\omega t)$. Real and imaginary parts contain the same variations, so it is possible to consider only the real part of such signal for studying relative sensor velocity.

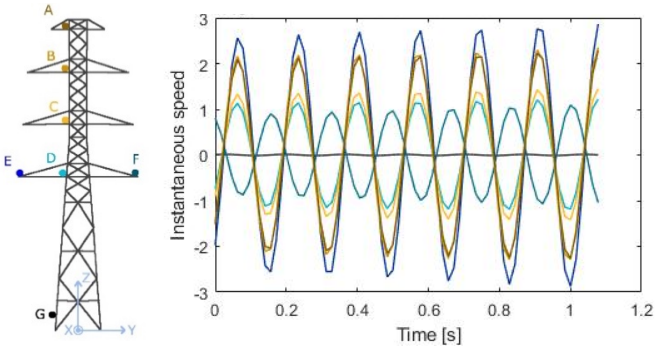


Figure 35: reconstruction of first torsion mode as time spectrum in transversal direction

It is even possible to build a GIF of the deformed shape from this filtered time signal to understand better how the structure is vibrating and identify the frame subgroups that are vibrating together.

4.4. Geometry capture

Although it seems surprising, most of the operators are not in possession of the manufacturing drawings of their towers. The tower needs to adapt to the ground, so they do not respect standard dimensions.

The external dimensions were measured by laser scanning with a Leica C10 device. The laser can browse its 360° environment. The principle is the same as ultrasound measurement: the device measures the time taken by the laser beam to come back to the emitter-receiver. It is possible to know this way the distance of the first object that the beam meets. Since a tower is a 3D object, despite its symmetry, it is recommended to scan it from different points of view to capture its full geometry. At least two stations are necessary if well located. Then, the different scan stations can be assembled in a dedicated software by specifying fixed points from one view to another. Several rotative targets whose center stays immobile are placed around the tower to act as such references.



Figure 36: Leica C10 Laser scan



Figure 37: Rotative target

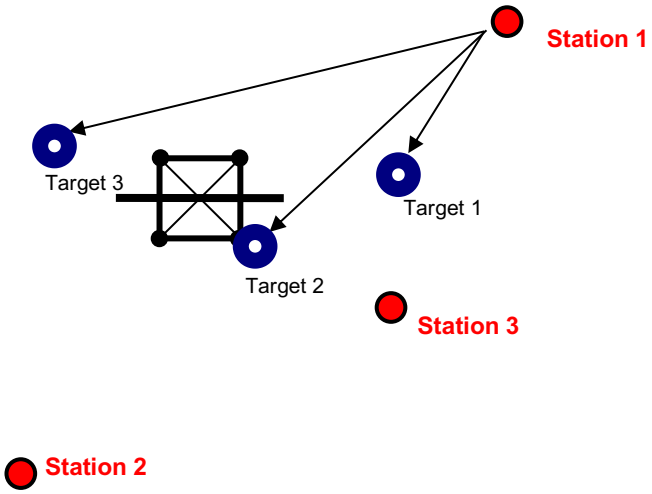


Figure 38: Example of target location and successive device positions

A point cloud can be imported directly from the scan device to a computer. After specifying the target location in each view, it is possible to combine all the point clouds to one and only Model Space view. This view is then imported true to scale to a drawing software. It is then very easy to extract the dimensions of the tower.

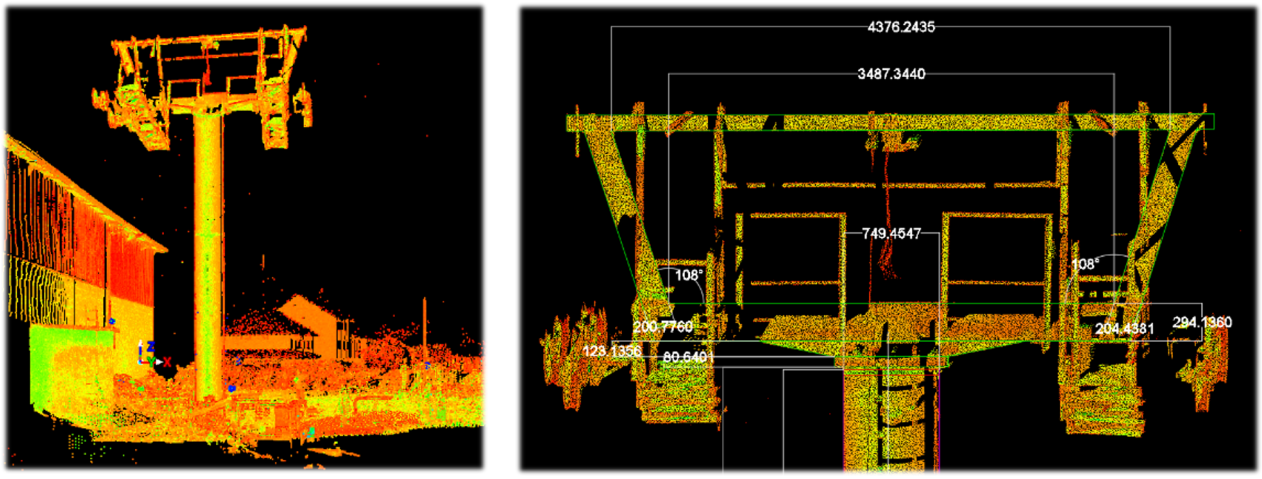


Figure 39: Dimensions of a ski-lift tower extracted from a point cloud through Autocad

The profile thickness was measured with an ultrasound probe. Galvanizing thickness can vary a little along the mast, so it necessary to calculate an average from at least five points.



Figure 40: ultrasound TT-100 device

4.5. Numerical model

4.5.1. Mathematical model

The ski-lift tower was modelled in exact dimensions through *Robot Structural Analysis* software. *Robot* performs a modal analysis by solving the matrix system of dynamic balance with no damping[2]. Basically, the software solves the following equation.

$$(K - \omega_i{}^2 M)U_i = 0$$

- K the structure stiffness matrix
- M the structure mass matrix
- ω_i the eigen pulse of mode i
- U_i the eigen vector of mode i

The number of modes to look for can be specified directly or by:

- The highest frequency to consider
- The lower limit of participating masses (%) to the inertia of each mode.

4.5.2. Discretization

The following finite element types are used in Robot Structural Analysis package:

- Beam element - standard 2-noded element
- Plane elements – 3 node triangles (T3) and 4 node quadrilaterals (Q4)
- Bending state – elements DKMT / DKMQ (Discrete Kirchoff – Mindlin Triangle / Quadrilateral)
- Membrane state – elements T3w and Q4w with corrected approximation of membrane state with respect to "drilling rotation"
- Curved Q4 elements – plate and membrane state are coupled together, and they cannot be separated as in plane elements

4.5.3. Modelling procedure

The modelling includes several steps:

1. First, it is necessary to define the 3D geometry by drawing the tower profile and assigning beam sections to every part of the tower. A material is assigned to every beam, here a standard steel. It is possible to create a material in the database. Assumption: every profile has a constant thickness.
2. Then, the external constraints are added.

3. Finally, the connections between the nodes are set by adding degrees of freedom. It is possible to define the connection between the ground and the tower.

   Assumptions: if the foundations are considered in good state, there is not any mobility at this location, zero degree of freedom. When unbolting the bottom, here we can add some degrees of freedom in rotation and eventually translation. The user has control of the six basic degrees of mobility of each connection.

   When the geometry of a piece is complex, it is also possible to replace it by a rigid connection and assign a mass at this location (*see fig. 30*).

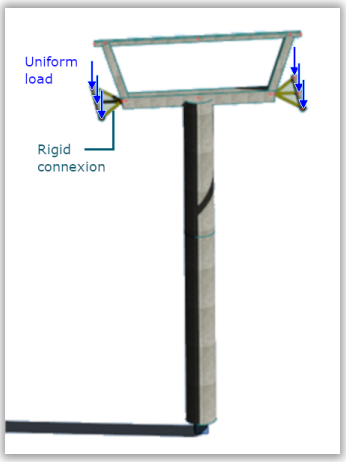


Figure 41: Structural model of a ski-lift tower in Robot Autodesk

4. Then, the user specifies a type of analysis. In our case, it is a "Modal analysis" that means every external constraint has to be converted into a corresponding modal mass. The software projects on the three axes the equivalent weight.

5. The results can now be computed and visualized. All the first modal frequencies are presented in a table and the respective deformed shapes can be visualized:

   - A dynamic way thanks to a short animation of a 3D-wireframe profile
   - As a 3D-image showing such wireframe while achieving its biggest displacement.

6. The maximum displacement in [mm] is also displayed: it helps to classify the modes among themselves and predict which ones might show a prominent peak on the frequency spectrum.

5. Results and analysis

The peak frequencies and related shapes depend mainly on the geometry of the structure, its material and its boundary conditions. A symmetric system, like these two towers, normally registers symmetric mode shapes. According to the following results, the bending modes occurs globally in the planes of symmetry of the structure when measuring vibrations in regular conditions.

5.1. Ski-lift tower

Curves and deformed shape are shown in appendix [6] and [8] for velocimeters, [7] for MEMS accelerometers and [9] for piezoelectric accelerometers. As expected, since the tower is supposed to be in good condition, when applying no load on the tower head the natural frequencies and related deformed shapes coincides quite well with the theory.

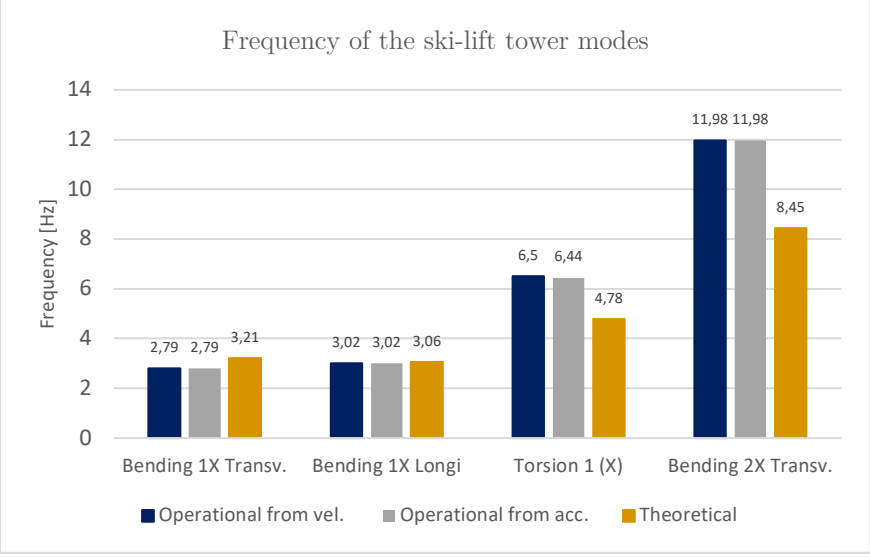


Figure 42: Mode shapes frequency extracted from velocimeters and MEMS accelerometers, compared to theoretical values computed on software, for the fully bolted ski-lift tower

Note: The piezoelectric accelerometers suffered an electronic issue during the recording of the tower with all bolts screwed and not loaded so that it was not possible to make a comparison with them. Moreover, since we had only three piezoelectric accelerometers, drawing deformed shape with them was not very relevant.

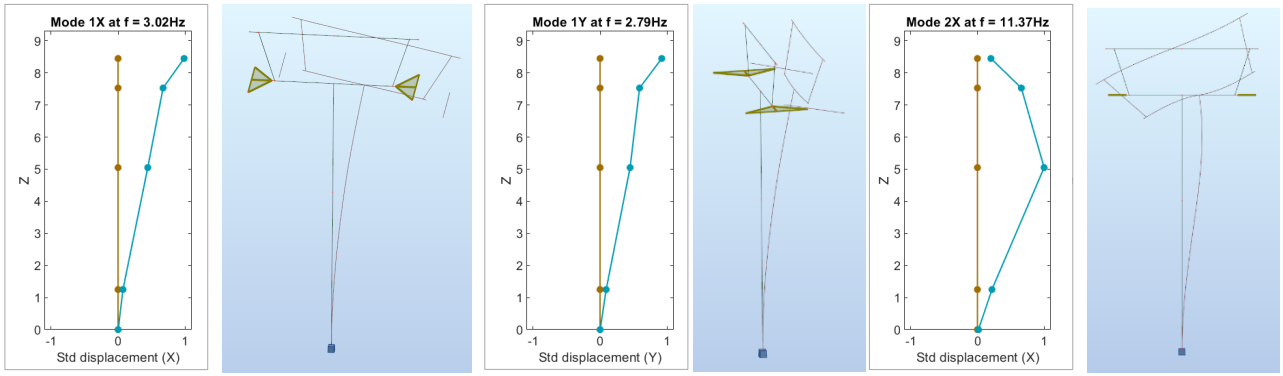


Figure 43: Comparison between theoretical tower first modes deformed shapes of the ski-lift tower and related experimental deformed shapes extracted from velocity measurements

The deformed shape measured by MEMS accelerometers and velocimeters, included in a same device, are not exactly the same, at least for the first bending modes. Actually, the MEMS accelerometers are expected to be noisy under 3Hz, so the velocimeters are considered more reliable inside this range. That being said, both sensors roughly show the same trend: at the bottom of the tower, the displacement is stronger than in the theoretical model:

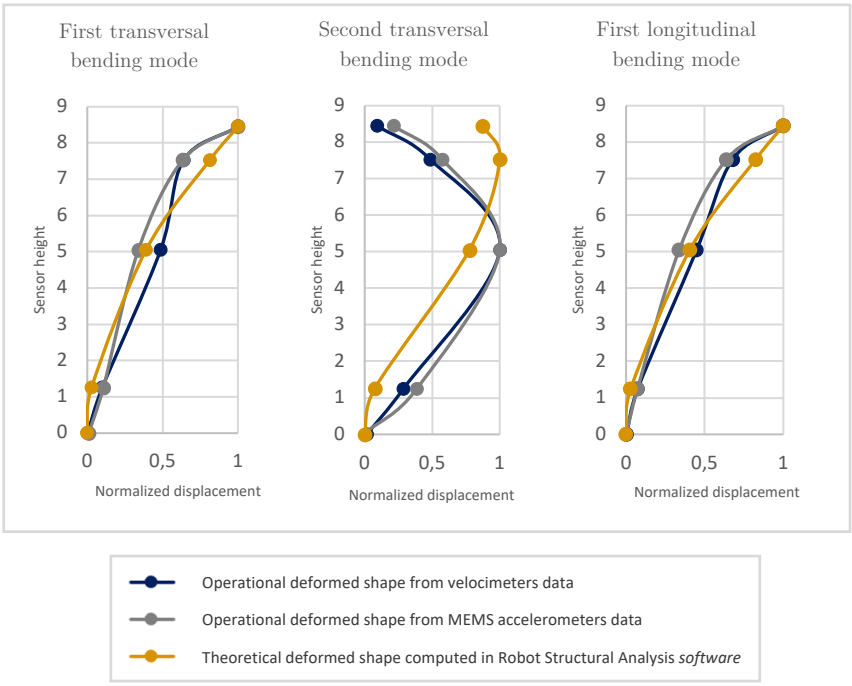


Figure 44: Comparison between the operational and theoretical deformed shapes for the fully bolted ski-lift tower

Depending on the model assumptions, the theoretical frequency value of natural modes can vary up to 20% without significant changes in deformed shapes. The trials performed on the ski-lift tower, without cables, can help us to adjust our theoretical model since we know such tower is supposed to be in good condition. In particular, the estimated mass distribution at the head of the tower has to be revised accurately. The second bending mode shape may help to adjust such model.

The different tests where embedding condition was modified show interesting results, whether for velocimeters or accelerometers. In particular, the number of frequency peaks in each direction can be modified. An exhaustive test result table is available in appendix [10].

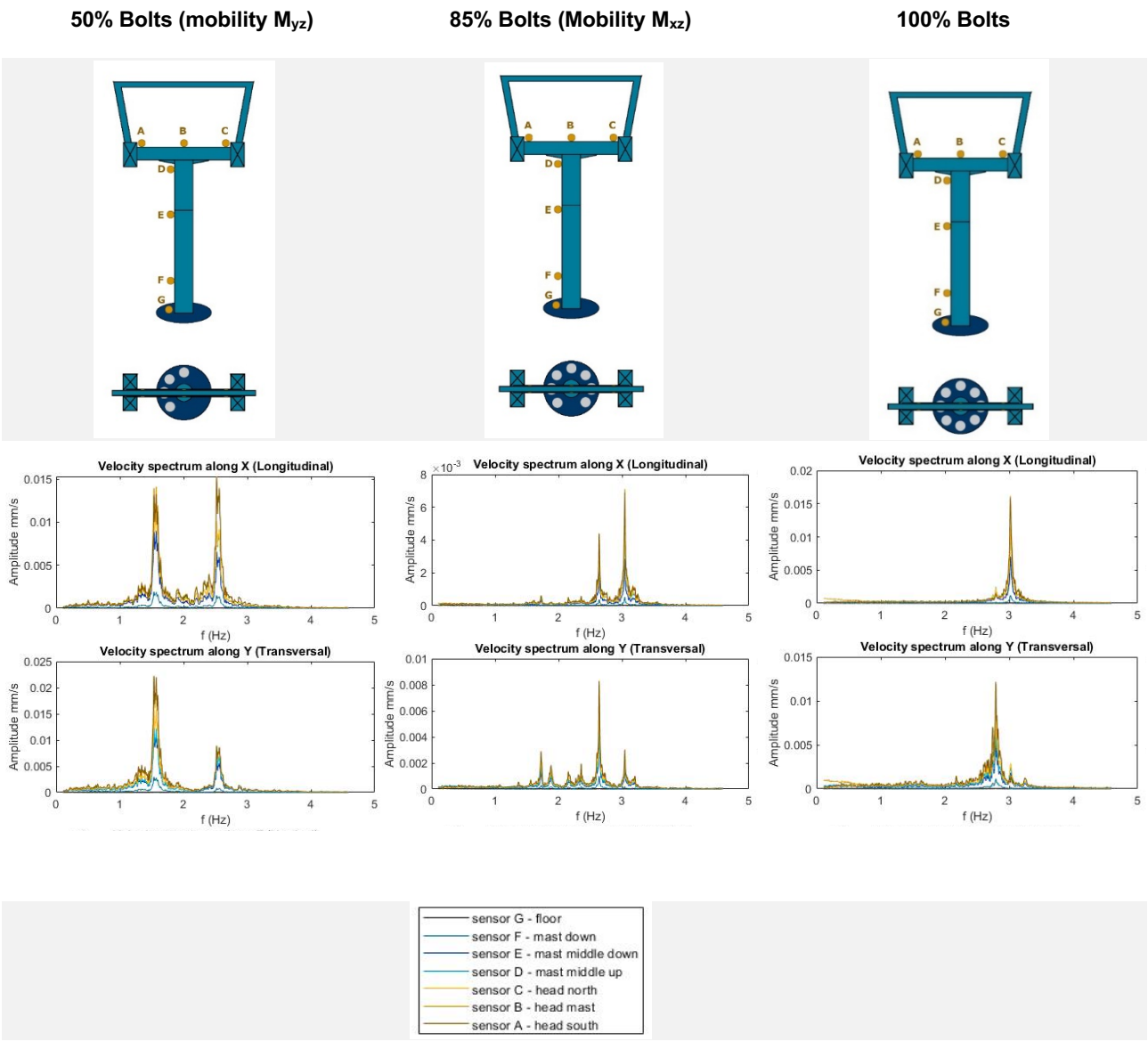


Figure 45: Velocity spectra for three types of foundation

When all the bolts are screwed, the spectrum shows, for first bending modes, one clear peak in each direction. When bolts are unscrewed, the modes that should occur in one specific direction are also visible in the perpendicular direction. Every directional mode seems to have been deflected or transformed into a circular mode. Besides, when unbolting screws in line direction, new secondary

peaks are appearing. These peaks disappears when a load is applied on the direction of remaining bolts. This phenomenon has no definitive explanation yet, but these new peaks could come from the resonance of a part of the tower.

Regarding to the load applied on cables, if the embedding is in good condition, the load does not act a lot on vibration modes. However, when some bolts are unscrewed, if a cable is tensed on the unscrewed side of the tower, it helps the tower to recover the main part of its stiffness.[8]

The following conclusions can be drawn from all the testing results on the ski-lift tower:

- A foundation in bad condition can imply bending modes that are not included in the planes of symmetry of the structure: a double peak appears in the spectra for the first mode in longitudinal and transversal directions.
- A foundation in bad condition can imply a decrease in first bending modes frequency.
- The load on top not always influences the frequency values of modes. A symmetrical load can slightly increase the frequency of the first modes when the foundation is in good condition. A unilateral load can hide the effect of a bad embedding at the bottom regarding to the frequency value.
- Measuring the frequency of torsion modes cannot help to detect foundations failures since it remains unchanged when unbolting the tower bottom.

5.2. Powerline tower

5.2.1. Velocimeter measurements

Power line towers have a complex structure with many frames. So, it is not possible to identify with confidence as many modes as for the ski-lift tower. Only the two first bending modes in each direction can be identified, and not even so precisely: there is not a unique peak but two or three very close to each other that shows a very similar deformed shape. Besides, not every of the four steel angles of the same tower shows exactly the same FFT spectrum.

Exhaustive results are available at appendix [11] and [12].

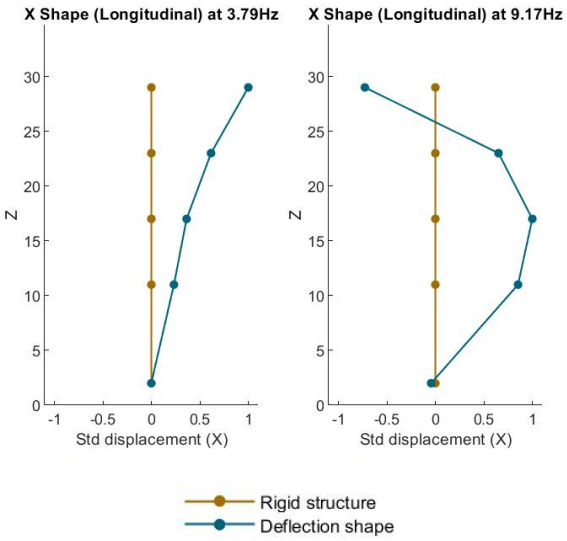


Figure 46: Probable first bending longitudinal mode shapes

Besides, each frame and each frame subgroup are likely to have their own vibrating modes. In addition, all the tower is not built with the same type of frames: the highest frames are thinner since they are used for security only. It is possible to see it in the deformed shape. For instance, the figure on the right, the measured deformed shape at 1.1Hz, shows a changing inertia around Z=25m.

This tower has not been modelled yet because geometric data was still missing. Thus, it is not possible to compare theory to measurements as it was done for the ski-lift tower.

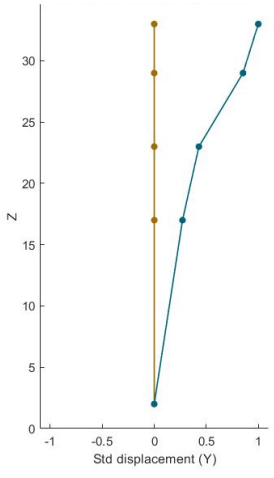


Figure 47: First transversal peak deformed shape of a power-line tower

The following frame describe the reconstructed temporal signal at such frequency.

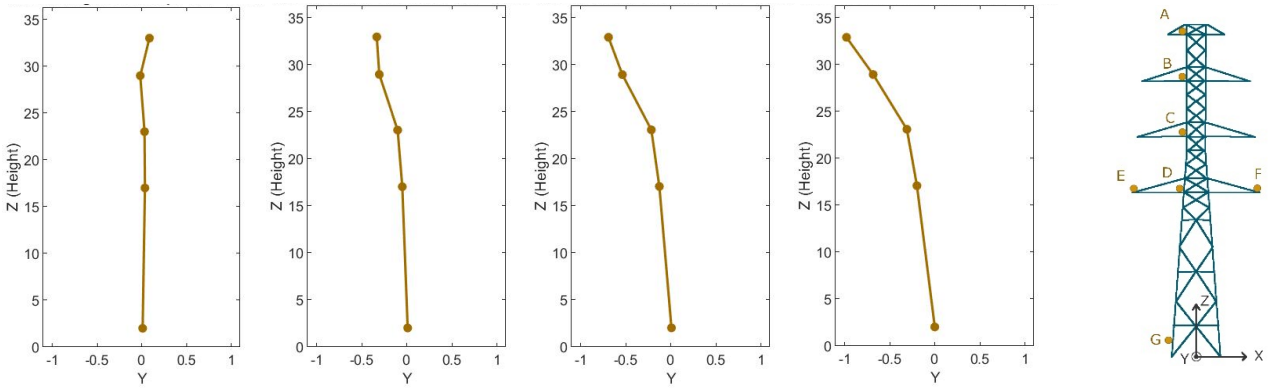


Figure 48: successive frames of vibration shape at 1.13Hz in transversal direction (perpendicular to line)

Such animation can help to figure out what means a $\frac{\pi}{2}$ phase difference between the curves of a sensor on the top and one at the middle. Here, the top of the tower is leading the movement and then the mast is following.

Soil-structure recordings [14] show that vibrations are transmitted to the ground just next to concrete slab since we register similar frequency peaks, but not several meters away. This can help for further test campaign to know how to arrange the sensors.

In such recording, we can note that the seismic excitation does not act as white noise at all: the FFT of the sensor on the ground far from the tower registers peaks every $n \cdot 5.6$ Hz, that suggests the presence of a rotating machine in the environment. When performing the testing, such excitation was not even perceptible.

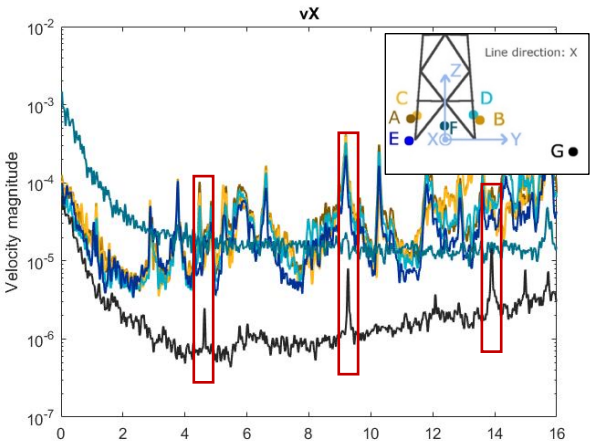


Figure 49: velocity frequency spectra along X

When watching the tower spectra for all sensors, the sensors located on the structure (ABCD) do not seem to register the same frequency peaks as the sensor on the ground far away (G), except for the 9.5Hz peak. As a matter of fact, the factor between ground (G) and structure (ABCD) vibrations at the bottom is very high (around 100). On the other hand, the sensor on the ground just next to the tower register a velocity very close to the ABCD sensors.

So, it would be incorrect building a transfer function considering only seismic excitation since wind and cables provides the main part of the input force applied to the tower.

Regarding to F sensor, located on the ground at the middle of the four tower feet, the recording shows completely incoherent signals in all directions: the geophone may have been blocked or suffered a perturbation.

Lastly, for such tower, it is possible to observe "ovalization modes" that were not perceptible on the ski-lift tower. At such mode, the powerline tower does not act like a beam anymore and suffer a compression of its mast in some of its frames. We can see frequency peaks on two steel angles at 4.5 and 5.5Hz.[4] [11] It is interesting to set sensors in the four feet simultaneously to confirm not every frame were following the same direction. In the recording performed near the floor, it was possible to watch slightly such trend [14], but it would have been more relevant to set sensors at a higher altitude. The fix location of the sensor A on the top was not very helpful either to analyze such synchronization since the movement is mostly present in the lower part of the tower.

5.2.2. MEMS accelerometers measurements

The MEMS accelerometers, included inside the velocimeter device, show globally the same frequency distribution as velocimeters. However, the related recorded phases seem to be erroneous since the recorded deformed shapes are completely incoherent, whatever the steel angle.

Another problem of such recordings was the influence of GPS signal reception. While receiving the GPS signal, at every second, some of the devices registered a disturbance along Z axis. This problem has been reported to the supplier who made modifications later on such devices.

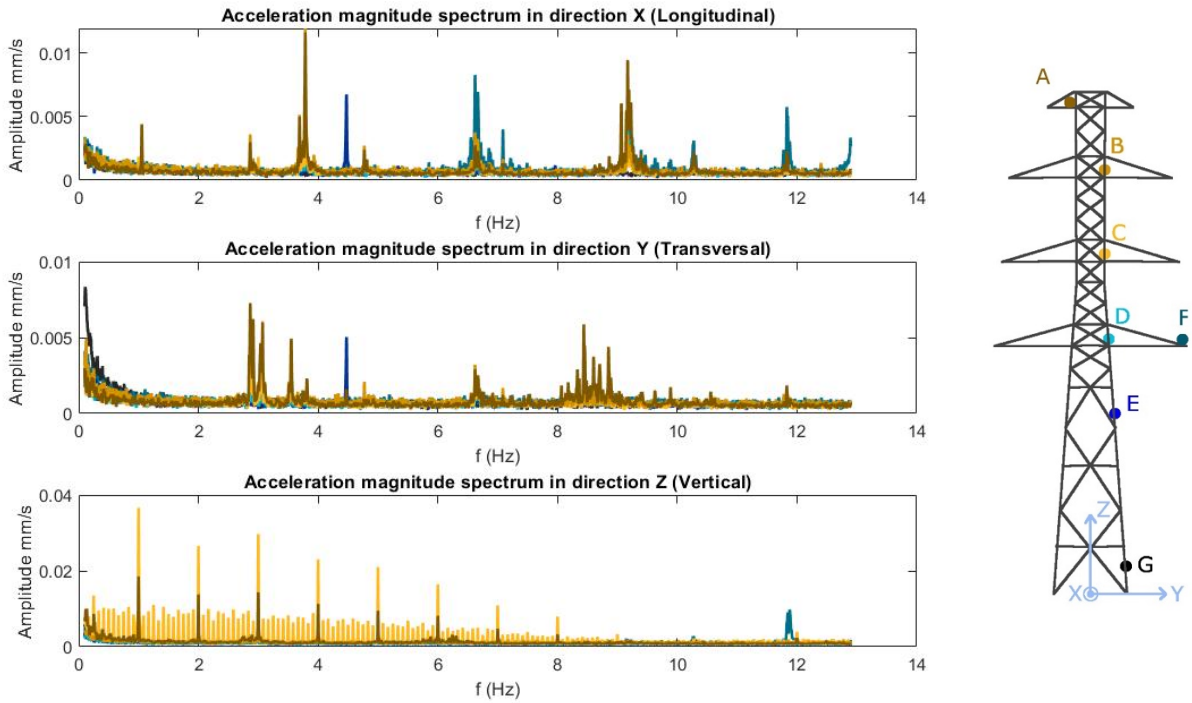


Figure 50: Acceleration frequency spectra for one the feet of the powerline tower

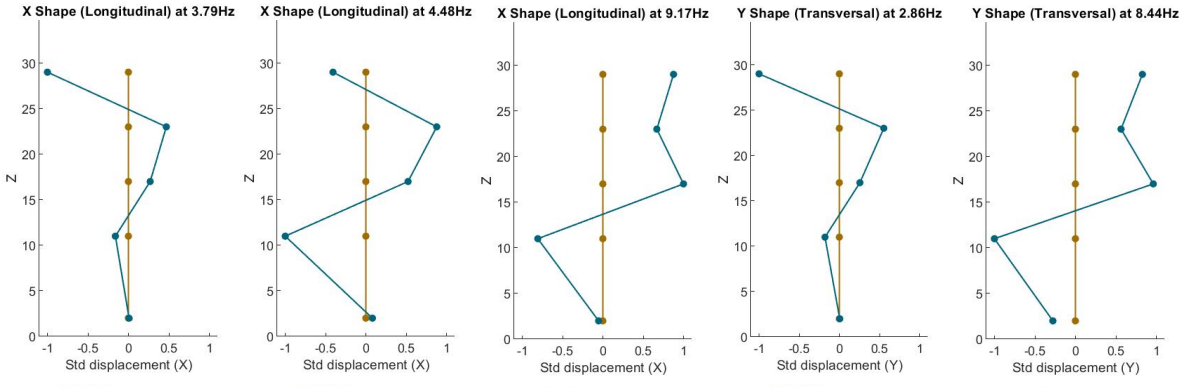


Figure 51: Deformed shapes extracted from MEMS accelerometers on the powerline tower

5.3. Signal distortion

5.3.1. Stability across the time

Some numeric tools can assess the signal stability across the time: autocorrelation function and spectrogram. The autocorrelation analyzes the similarity between a signal and delayed copies of itself. It gives information about the periodicity and the stability across the time.

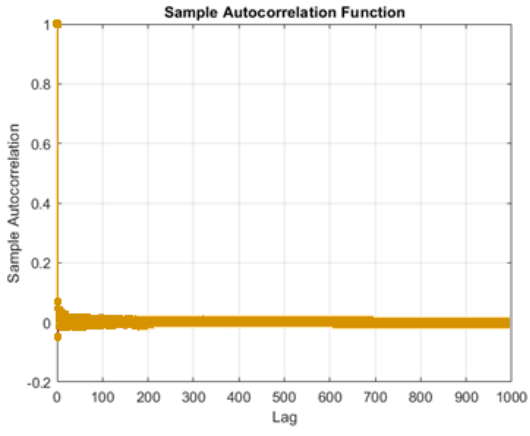


Figure 53: Noisy signal autocorrelation

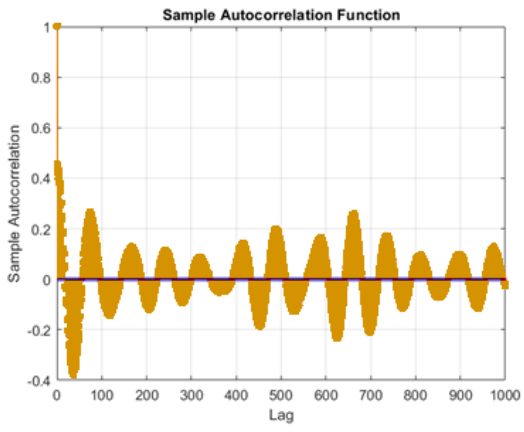


Figure 52: Periodical signal autocorrelation

It is possible to detect this way the less autocorrelated windows or the windows that are less similar to the others. These noisy windows can be removed from time data by setting a value of zero instead of all the velocity data of the window (zero padding process). Then, the remaining parts of the signal have to be windowed with a hamming or hanning filter to limit the distortions implied by setting a part of the signal to zero. Without such filter, setting down to zero parts of the signal would imply a convolution of the signal with the heavyside function and create side lobe effects. Hanning and hamming filters reduce the prominence of such lobes.

Another way to evaluate periodical stability is the Welch spectrogram. It provides the frequency composition of a signal across the time. Basically, the Welch periodogram performs a FFT on very little windows of time signal and displays as a picture such evolution.

When a high magnitude is repeated at some frequency all over the data, the spectrogram gets red. This technique is usually used to distinguish a constant excitation from a punctual one.

The picture on the right describes the frequential composition of the signal received at the top of the ski-lift tower, at the center.

The frequency resolution of a spectrogram is depending on the window size and the recorded time. In such example, the window size is 10 seconds with a 66% overlap.

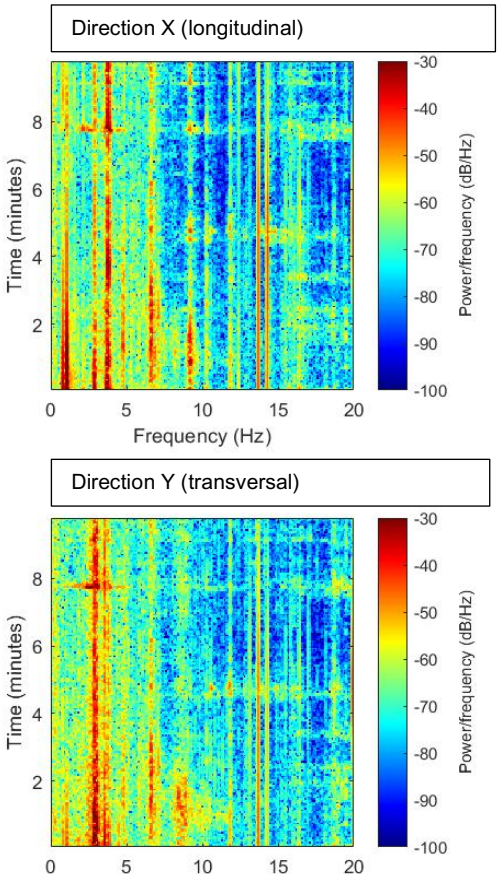


Figure 54: Spectrogram of the sensor located at the top of the powerline tower

We can see punctual excitation at times 4'30" and 7'50" which could be a shock related to seismic excitation since all the frequencies seem to be present on the spectra. This would be thus the "purest" instants to consider the structure response to white noise. Such analysis was very helpful to differentiate noise disturbance from mode shapes when there were many close frequency peaks on the powerline tower. Here, thanks to the shock suffered at 7'50", we can see estimate the first X-mode shape around 3.7Hz and the first Y-mode shape around 3Hz.

The mode shapes can sometimes help to identify which peak is a bending mode shape and which is not, but in the case of the powerline tower it was not possible because they were all very similar.

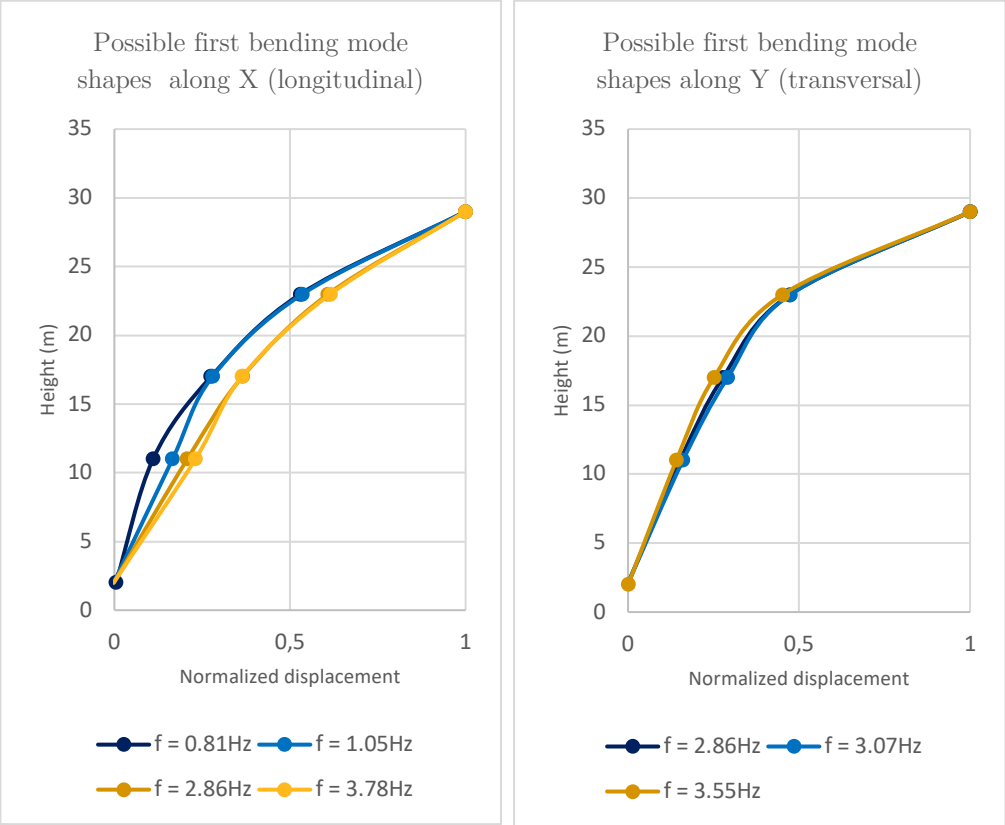


Figure 55: Mode shapes related to the first frequency peaks of one of the four angle iron of the powerline tower

It is also interesting to compare each of the four main frames of the tower to underline a frequency that always appear. Here, the main peaks were not always appearing at the same frequency for every frames.[11]

The frequency peaks that are not due to a natural mode can be implied by the resonance of a component which is linked to the system. In particular, the last spectrogram shows a frequency comb over 13Hz with peaks regularly spaced. Such a periodicity whose fundamental frequency is around 1Hz could eventually come from the cable resonance [53]. As a matter of fact, such peaks are strongly visible for the lateral sensor F, which is linked to the cable.

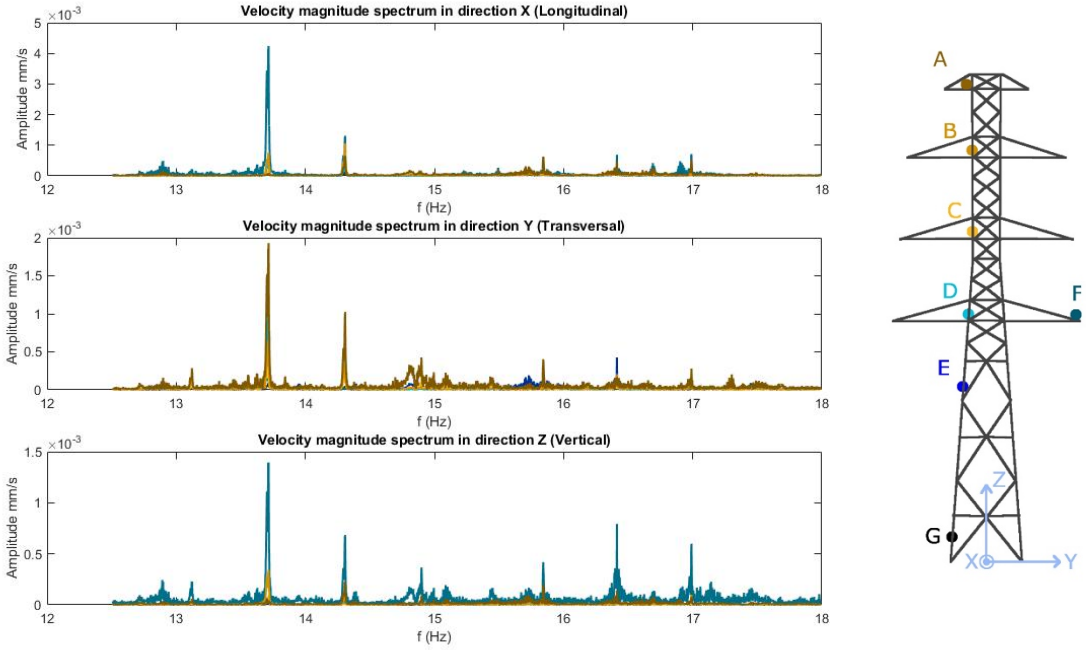


Figure 56: Frequency spectra for one of the frames

5.3.2. Cable influence

It is possible to determine the theoretical fundamental frequency of a cable by measuring the stress it supports: $\boldsymbol{f_0 = \frac{1}{2L} \cdot \sqrt{\frac{T}{\mu}}}$

L *the distance between both towers*

T *the tension stress in the cable at the fixation point*

μ *the linear density of the cable*

We measured the vibration on a cable which was linked to a structure thanks to isolators. The precise modelling of the system {cable + isolators} will be performed further in the company.

As a first observation, we can suppose that the fundamental frequency of this couple is mainly defined by the cable tension stress. The isolators are considered as solid objects connected to the towers in a rigid way. The cable describes a parabola defined by the distances L and h in the picture.

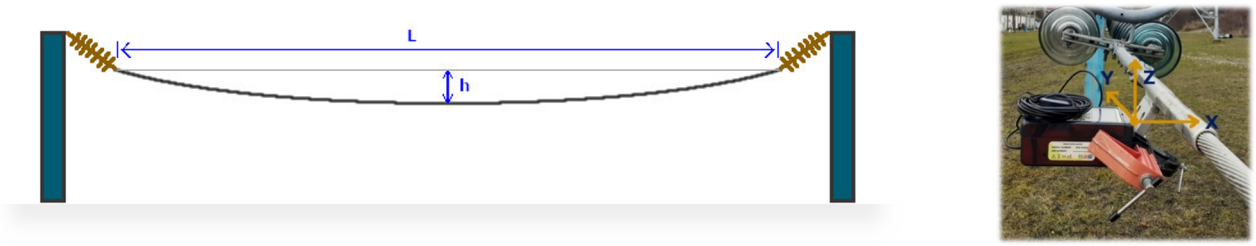


Figure 57: High voltage cable disposition at ground level

Geometric distances can be extracted from a laser scanning. Since the tension stress is mainly due to the cable dead weight, we can write it:

$\boldsymbol{T = a \cdot \mu \cdot g}$

g *the universal gravitation constant*

$\boldsymbol{a = \frac{\frac{1}{4}L^2 - h^2}{2h}}$ *a geometric parameter considering the cable as a parabola with* **h** *its vertical deflection*

Therefore, the fundamental frequency can be calculated with only geometric information:

$$\boldsymbol{f_0 = \frac{1}{2L} \cdot \sqrt{a \cdot g}}$$

Thanks to laser scanning measurements, we can try to approximate the parameter a:

$a \approx \frac{0.25 \cdot 43.2^2 - 0.14^2}{2 \cdot 0.14} = 1663$ m

$f_0 \approx \frac{1}{2 \cdot 43.2} \cdot \sqrt{1663 \cdot 9.81}$ **=1.47 Hz**

The experimental spectrum shows a frequency peak around **1.17 Hz** for the first mode perpendicular to cable (directions X and Z). [16]

The operational frequency is a little lower than the theoretical one. This can be explained by the hypothesis regarding to the isolators: since they are actually not perfectly rigidly connected to the structure, they are moving slightly with the cable. It is quite analog to the natural frequency drop of a tower while unscrewing its foundation.

As a comparison, if we would have considered the system {cables + isolators} as a chain, we would have obtained:

$a \approx \frac{0.25 \cdot 50.9^2 - 0.47^2}{2 \cdot 0.47} = 689$ m, *considering the system describes an ideal parabola*

$f_0 \approx \frac{1}{2 \cdot 50.9} \cdot \sqrt{689 \cdot 9.81} = 0.81$ **Hz**

Since we are measuring the frequency of the couple, we can check that 0.81 Hz < 1.17 Hz < 1.47 Hz.

Beyond checking the magnitude order of such a cable natural frequency, these tests were also performed to overview its vibration behavior, especially the repeatability of peaks at the multiples of f_0. Actually, even drawing the spectra with a logarithmic scale, the cable velocity does not show frequency peaks at $n \cdot f_0$.

It is difficult to conclude about the influence of such cable resonance on the tower spectrum since the excitation provided here did not come from the wind blowing. Moreover, the magnitude of the mode is probably not linked by a linear relation to the force input to the tower at anchoring location.

It would be relevant to plan further tests with a cable in operating conditions and with a smaller and lighter device such as a MEMS accelerometer alone.

While calculating the natural frequency of the cables anchored at the tested tower [15], we find:

- For the cable anchored near sensor F: $f_0 = \frac{1}{2 \cdot 41.2} \cdot \sqrt{\frac{0.755 \cdot 41.2 - 0.755^2}{2 \cdot 0.755} \cdot 9.81} = \mathbf{0.42Hz}$
- For the cable anchored at sensor B height: $f_0 = \frac{1}{2 \cdot 42.8} \cdot \sqrt{\frac{1.096 \cdot 42.8 - 1.096^2}{2 \cdot 1.096} \cdot 9.81} = \mathbf{0.40Hz}$

In almost every spectrum of the tower, we can notice that F sensor, located just next to a cable anchoring, is often recording vibration in low frequency (between 0.2 and 0.4 Hz especially)[11]. However, it is not enough to say that such vibrations of the cables are getting transmitted to the structure.

5.3.3. bracket influence

A quick test was performed to determinate the bracket modes of vibration. Two sensors were fixed on a ski-lift tower on their support with straps at the same height. An operator was hitting one of the supports during the whole recording. The spectra in the three directions show resonance frequencies mainly between 35 and 65Hz.[17] Then, this should not disturb our measurements since the first structure mode shapes occurs between 1 and 20Hz.

Though, another periodicity is also visible in this recording. Its fundamental frequency is around 0.3Hz and it is repeated for every multiple of it. In some recordings performed on the tower in ambient noise,

similar peaks could sometimes be visible for sensors fixed with a support but never with sensors laid directly on a beam.

Lastly, a testing was performed while hitting the tower every 3-4 seconds. If such protocol was necessary for piezoelectric accelerometers, it was not accurate for the other device. As a matter of fact, the fixation system of the device to the structure can introduce some disturbance: we can see the spectra of both velocimeters, and MEMS accelerometers are very noisy in these conditions. Such noise is describing something similar to the spectra obtained by hitting directly the bracket.[17]

These noise disturbances can come from the support itself but also from the stability of the sensor in the support for example. The brackets are handmade so there are not perfectly plane, but the sensor was placed on it with three points of pressure.

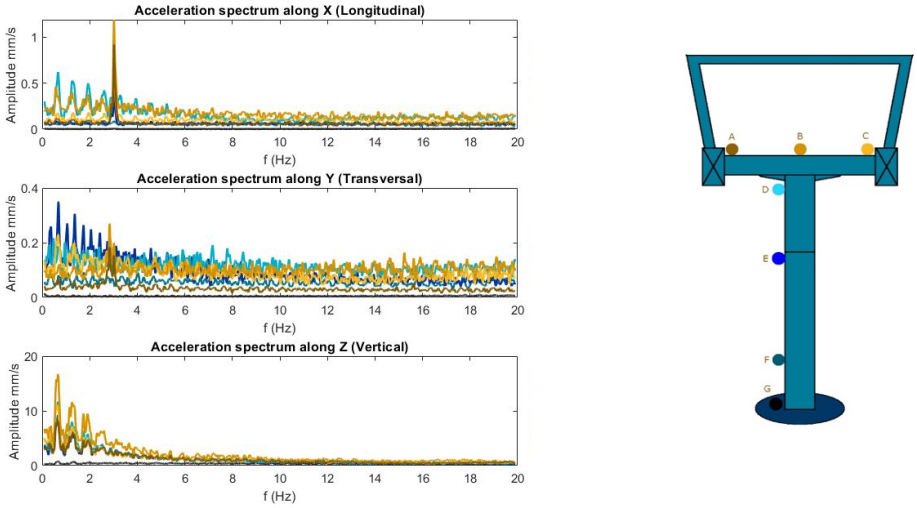


Figure 58: Acceleration spectra of the ski-lift tower while hitting it

As we can see in the temporal signal of such testing, the velocimeters seem to lose their stability when a shock is suffered.

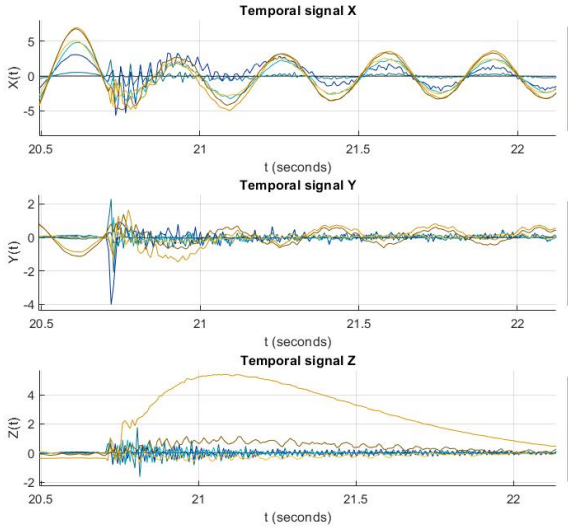


Figure 59: temporal velocity spectra of the ski-lift tower while hitting it

5.3.4. Sensor influence

The results from velocimeters and piezoelectric accelerometers lead almost to the same results. However, only the accelerometer recordings showed peaks at $12.5 \cdot n$. These peaks may come from the sensor. They were not considered in the analysis.

Some tests were conducted in order to compare the velocimeters SURICAT [18]– used for all the tests – with its premium version TROMINO[19]. The two sensors were placed at the same location and both of them recorded the same spectra.

6. Conclusions

6.1. Technical conclusions

A **mode shape analysis** performed on high metallic towers can provide valuable **structural information**. The **ambient noise** provides enough energy to the tower for it to vibrate. Several velocimeters located along the tower can be **synchronized** to assess the **global structural behavior**. These experimental measurements allow to perform an assessment of the structure condition many years after building the tower.

A code based on FFT implemented in Matlab was utilized **to compute the frequency spectrum of the tower response to ambient vibrations and visualize the deformed shapes at each peak**.

Comparing measurements on a flawed structure with the numerical model of a pristine tower the following **failures (weakness) can be detected**:

- if the **natural frequency of the first mode shape** is **abnormally low,** the **foundation might be in bad condition.**
- if **a mode shape occurs in a deviated direction or provides a circular movement,** the **foundation might be in bad condition.**

In this sense, **local issues** can be detected by assessing the **global movements** of the structure. The ideal numerical model can be modified to mimic the response of the structure recorded in the experiments by **relaxing some of the boundary conditions**.

The **ski-lift towers** generally have one ground **foundation** and are made of a few welded pipes. These towers are quite **robust** and to a good approximation can be considered as **one-piece structure** when

they are in good condition. In case of abnormal value of modal parameters, the **possible origins** of the issue **are limited** (foundation, welding or bolted assembly). On the contrary, the **power line towers** have **four ground foundations** and are **made of many interconnected frames**. **Each subassembly implies more degrees of freedom and thus more vibrational modes**.

The main limitation of the present methodology is the **lack of white noise in the input excitation of the tower**. **Most of the ambient noise vibration is convoluted by the cable resonance before being applied to the tower**. So, **the tower receives a frequency comb signal**, i.e., not all the frequencies are excited in the same way. Since the force input due to the cable vibration is not measured – and it would be difficult to measure – **a precise assessment is a complex process since it is difficult to discern whether a peak is due to a natural mode of the tower itself or due to a huge excitation at such frequency produced by natural mode of the cable. The determination of the exact transfer function of a tower would require more recording points and control of the excitation signal. This** implies a logistic not available during the period of this internship.

Finally, it would be **necessary to perform such testing** with other towers and more sensors to **build a significant data base to have more conclusive evaluations**.

6.2. Perspectives and future work

6.2.1. Deeper study of power-line towers

The tested high-power line tower has not been modelled yet. Such model will make possible to compare numerical predictions with measurements.

6.2.2. Effect of an intentional degradation on the tower mast bolted/welded connections

Experimental measurements were performed with bolted and unbolted ground connections on the ski-lift tower. However, a foundation in bad condition is not the only defect on such structures.

For instance, it would be interesting to study the effect of a defected welding. Such testing is quite difficult to perform in a non-destructive way, so it is more convenient to performed a posteriori evaluation of a damaged structure.

6.2.3. Testing with pseudo-controlled excitation method

As we could see in the power-line tower measurements[5.3.2] and in many internal reports[53][54][56][57], when a tower is connected to line cables their resonance produced by wind excitation represents the main energy source to the tower. It is not convenient to perform the tests without cables on site for obvious reasons. It would be interesting to provide a huge amount of energy to the tower by producing an impact load for instance by dropping a heavy mass attached to the top of the tower by a cable. Such impact load would act as a seismic excitation. It would probably minimize the effect of the cables.

6.2.4. Numerical predictions as a tool to identify natural modes from experimental signals

Among the different peaks that can be visible in the frequency spectrum, not all of them are due to a vibrational mode. As explained above, the response of the tower can be influenced by the excitation, especially if the ambient vibration does not exactly behave as white noise. It is necessary then to compare the deformed shapes obtained in the peaks range. The mode can be identified if it is similar enough to the numerical shape mode. Thus, it would be very useful to develop algorithms to study such correlation by performing a scalar product between the operational deflection shape at each

frequency range and the numerical mode shapes. This algorithm will provide a coherence indicator that would help to identify the frequency of these modes.

6.2.5. Comparison with the results from other non-destructive techniques

The non-destructive techniques generally provide huge but incomplete information, that is why it is recommended to combine the results of different Non-Destructive Techniques before drawing definitive conclusions regarding to the condition of a system. In our case, the laser scanning point can provide information on permanent deformations. This study is planned to be conducted in the following months.

An additional future project is to perform vibration measurements of three towers. A comparative study can also be conducted where the structures could be analyzed by other companies with another type of NDT.

6.2.6. Uncertainty of measurements assessment

The numerical model includes assumptions, and the experimental measurements always contain errors. How significant could be a measurement error and uncertainties on results of a mechanical failure assessment? In other words, if there is a structural issue in the tower, could it be possible to detect it accurately? Would a frequency or shape incoherence be caused by a model/device error?

It is important to determine the statistical error on measurements by a careful design of the experiments including variables such as the locations of the sensors, the threshold of “abnormality”, environmental parameters like temperature, among others. It would be interesting to perform measurement on a same tower through different climate conditions, at different seasons of the year.

6.3. Personal experience

This internship was a very fruitful experience on a research project in a private company. I was able to benefit from a field experience, being involved in some parts of software development, teamwork, interaction contacts with partner companies and researchers in the lab. I learned a lot and got the opportunity to be creative. I was asked to understand at fast pace specific notions of vibrations by self-study.

In my personal opinion, such a research project requires many years of preparation before being totally operational. The analysis tool was not ready to be deployed without a more exhaustive development process: sometimes the pressure to obtain results is not compatible with research objectives.

By writing such an academic report, in addition to my internship report, I could really figure out the difference between the industrial and academic approaches on a project. An employee is expected to be quickly operational and productive, starting from the previous works and assuming that the suggested tools are accurate, whereas a student is invited to question every assumption, every protocol, even every software and understand how does work every analytic tool.

Finally, this internship was very rewarding for me because I could understand what matters to me as an engineer, beyond the technical aspects.

7. Bibliography

7.1. Theoretical basics

1. *But what is the Fourier Transform?* A visual introduction. (2018, 26th of January). YouTube. https://www.youtube.com/watch?v=spUNpyF58BY
2. Heideman, Michael T.; Johnson, Don H.; Burrus, Charles Sidney (1984). *Gauss and the history of the fast Fourier transform*. IEEE ASSP Magazine.
3. Van Loan, Charles (1992). *Computational Frameworks for the Fast Fourier Transform*. SIAM.
4. *Transformées de Fourier usuelles* — Wikiversité. (2021, 25 mai). Transformées de Fourier usuelles. https://fr.wikiversity.org/wiki/Transform%C3%A9es_de_Fourier_usuelles
5. Halliday, Resnick & Walker 2005, p. 324.
6. Wikipedia contributors. 2021. *Harmonic oscillator*. Wikipedia.

   https://en.wikipedia.org/wiki/Harmonic_oscillator#Driven_harmonic_oscillators
7. *GM4 MEAVS - Vibration Analysis of Structures*. Nicolas Totaro. INSA Lyon, Mechanical department, 2020.
8. *GM3 VIBAC – Vibrations des systèmes mécaniques, modèles discrets*. Régis Dufour, Eric Châtelet. INSA Lyon, Mechanical department, 2017.
9. *Yang, B. (2005). Stress, Strain, and Structural Dynamics: An Interactive Handbook of Formulas, Solutions, and MATLAB Toolboxes. Academic Press.*
10. http://perso.univ-lemans.fr/~jcpascal/Cours/ENSIM2A_Vibrations&Acoustique_1.pdf
11. https://www.modalshop.com/techlibrary/Fundamentals%20of%20Modal%20Testing.pdf
12. https://www.uml.edu/docs/Modal_Space_Articles_1998-2014_17years_MACL_tcm18-189938.pdf
13. https://blog.prosig.com/2009/10/19/a-simple-frequency-response-function/
14. https://videos.mentor-cdn.com/mgc/videos/5400/381c214d-89be-4066-afa8-1f25f5a76344-en-US-video.mp4

15. Randall RB, Smith W, Antoni J. *A survey of the application of the cepstrum to structural modal analysis*. Mech Syst Signal Process. 1 mars 2019; 118:716-741

16. LMS International. LMS. *Theory and Background*. 2000. 361 p

17. http://math.univ-lille1.fr/~bodin/geometrie/ch_chainette.pdf

18. *Frequency-response functions for modal analysis* - MATLAB - MathWorks France. (2021). modalfrf. https://fr.mathworks.com/help/signal/ref/modalfrf.html

19. *Principes adoptés dans l'analyse modale de la structure*. (2020, 24th of July). Robot Structural Analysis Products | Autodesk Knowledge Network.

    https://knowledge.autodesk.com/fr/support/robot-structural-analysis-products/learn-explore/caas/CloudHelp/cloudhelp/2019/FRA/RSAPRO-UsersGuide/files/GUID-3400C9A4-F47F-4A7F-9B67-66BEE7B9105A-htm.html

20. *Analyse modale avec la prise en compte des efforts statiques - description et exemple*. (2015, 11th of December). Robot Structural Analysis Products | Autodesk Knowledge Network.

    https://knowledge.autodesk.com/fr/support/robot-structural-analysis-products/learn-explore/caas/CloudHelp/cloudhelp/2016/FRA/RSAPRO-UsersGuide/files/GUID-B3450A84-E078-484E-80B9-3AA0482F3699-htm.html

21. Rao Ph.D. Case Western Reserve University Cleveland OH, Singiresu S. (2017). *The Finite Element Method in Engineering* (6e éd.). Butterworth-Heinemann.

22. *What types of finite elements are used in Robot Structural Analysis*. (2020, 15 th of September). Robot Structural Analysis Products | Autodesk Knowledge Network.

    https://knowledge.autodesk.com/support/robot-structural-analysis-products/troubleshooting/caas/sfdcarticles/sfdcarticles/ROBOT-what-types-of-finite-elements-are-used-in-the-program.html

23. http://perso.univ-lemans.fr/~jcpascal/Cours/ENSIM2A_Vibrations&Acoustique_1.pdf

24. M. A. Laughton; D.F. Warne (27 September 2002). Electrical Engineer's Reference Book (16 ed.). Newnes. pp. 14/9–14/10. ISBN 978-0-08-052354-5

7.2. State of the art

25. https://en.wikipedia.org/wiki/Ultrasonic_testing#/media/File:UT_principe.svg
26. Wikipedia contributors. (2021, 1 juillet). *Ultrasonic testing*. Wikipedia.
27. Perez, Nicolás. (2011). *Monitoring of corrosion in pipes using an array of ultrasound transducers*.
28. Corneloup, G., & Gueudré, C. (2016). *Le contrôle non destructif et la contrôlabilité des matériaux et structures (METIS LyonTech) (French Edition)* (Vol. 1). PU POLYTECHNIQUE.
29. *Dye Penetrant Inspection*. (2014, 4 mars). YouTube. https://www.youtube.com/watch?v=xEK-c1pkTUI
30. Sölken, W. (2008–2021). *Non Destructive Testing - Dye Penetrant Inspection*. Wermac.Org. http://www.wermac.org/others/ndt_dyepenetrant.html
31. Singh, R. (2020). *Applied Welding Engineering : Processes, Codes, and Standards* (3e éd.). Butterworth-Heinemann. https://doi.org/10.1016/B978-0-12-821348-3.00026-4
32. https://www.suragus.com/en/technology/eddy-current/
33. http://www.joe.buckley.net/papers/eddyc.pdf
34. Carlos Pairazaman, Sara Keller, Charles Buynak. (2000). A Third Generation Robotic Eddy Current System for the Inspection of gas Turbine Engine Components. *15th World Conference on Nondestructive Testing, Roma (Italy)*. Published.
35. https://mistrasgroup.fr/prestation-de-service/controle-non-destructif/ultrasons-semi-automatises/lsi/
36. https://www.fprimec.com/ultrasonic-testing-of-concrete/
37. https://www.fprimec.com/case-studies/non-destructive-evaluation-of-transmission-line-foundation/
38. https://www.jf-strainstall.com/load-monitoring-products/specialist-testing-equipment/bgcmap-rate-corrosion-tester/
39. Bhowmik, Er. Chiranjit & Chakraborti, Prasun. (2020). *Analytical and Experimental Modal Analysis of Electrical Transmission Tower to Study the Dynamic Characteristics and Behaviors*. KSCE Journal of Civil Engineering. 24. 931-942. 10.1007/s12205-020-1563-3.

40. https://www.fprimec.com/pile-integrity-test/

41. https://moho.world/en/suricat/

42. https://www.kinectrics.com/Case-Studies/Pages/Tower-Vibration-Monitoring.aspx

43. Mougenot, D. (s. d.). *How digital sensors compare to geophones?* Sercel.com. https://www.sercel.com/products/Lists/ProductPublication/Sercel-digital-geophone-1.pdf

44. Sandro D. Rescinho Amador, Luis A. Conte Mendes Veloso Remo Magalhães De Souza, And Jean Rodrigo F. Aguilera. (2006). *Full-scale experimental modal analysis of an overhead transmission line tower crossing Guamá river in the Amazon region.* The 13th International Congress on Sound and Vibration. Published

45. https://www.digikey.fr/fr/articles/what-you-need-to-know-about-vibration-sensors

46. Magnifying motion. (2015, 23 avril). YouTube. https://www.youtube.com/watch?v=MYp298fhlzk

7.3. Vibration analysis Applied to concrete cases

47. François Dunand. *Pertinence du bruit de fond sismique pour la caractérisation dynamique et l'aide au diagnostic sismique des structures de génie civil.* Géophysique [physics.geo-ph]. Université Joseph-Fourier - Grenoble I, 2005. Français. tel-00335885

48. Ali Mikael. *Evaluation des paramètres physiques des bâtiments : amortissement, fréquence et modes de comportement des structures de génie civil : approche expérimentale.* Sciences de la Terre. Université de Grenoble, 2011. Français. NNT : 2011GRENU016. tel-00597269

49. Combet, P Jaussaud, Nadine Martin. *MODÉLISATION : DE LA PHYSIQUE AU TRAITEMENT DU SIGNAL Modèles vibratoires dans les remontées mécaniques.* La Revue de l'Electricité et de l'Electronique, Société de l'Électricité, de l'Électronique et des Technologies de l'Information et de la Communication, 2003. hal-01767315

50. Sherif Beskhyroun, Niusha Navabian, Liam Wotherspoon, Quincy Ma. Journal of Building Engineering. *Dynamic behaviour of a 13-story reinforced concrete building under ambient vibration, forced vibration, and earthquake excitation*

51. A. De Vivo, C. Brutti, J.L. Leofanti. *Modal shape identification of large structure exposed to wind excitation by operational modal analysis technique.* Mechanical Systems and Signal Processing. Volume 39, Issues 1–2, 2013, Pages 195-206.

52. Jean-Luc Chatelain, Bertrand Guillier, Philippe Gueguen, J. Frechet, Jacques Sarrault. *Ambient vibration recording for single-station, array and building studies made simple: CitySharK II.* Inter- national Journal of Geosciences, Scientific Research 2012, 3, pp.1168-1175. 10.4236/ijg.2012.326118 . hal-00790355

7.4. Internal documentation

53. Adrien Marswick. Projet Recherche & Ingénierie PRI-2019S9-VIL24-SA401. *Analyse critique et perspectives d'une méthode d'évaluation de la vulnérabilité des ouvrages par analyse vibratoire.* 2020.

54. Aim Sarrasola. *Rapport d'investigations EVE TSF Chamois 2018. 2019* Report No.: P.0159147.A.24.001.B.

55. Aim Sarrasola. *Mode opératoire P12 ARGIA AKALE* 05-09-2019

56. Miage. Sarrasola. 18120. *Rapport d'interventions EVE TSF Crans Montana 2018. Funitel plaine morte. Pylône P2. Mesure des paramètres dynamiques du pylône.*

57. Miage. Sarrasola. P.0113692.D.24-001 B *Rapport d'investigations EVE Ligne Vallorcine – La Batiaz sur le pylône P2,. Pour Swissgrid. Rapport de synthèse.*

8. Appendix

[1] Acquisition on a ski-lift tower with velocimeters in ambient noise







[2] Acquisition on a ski-lift tower with accelerometers with a woody mass to excite the structure







[3] CHTF (high voltage training academy)



[4] Acquisition on a power line tower with velocimeters in ambient noise



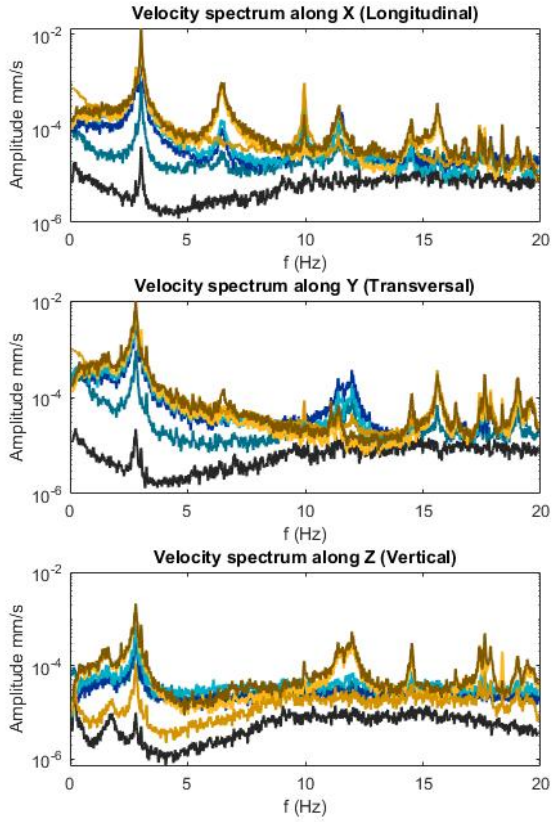
[5] Acquisition with velocimeters on a typical cable of power lines, ref. cable PASTEL 228

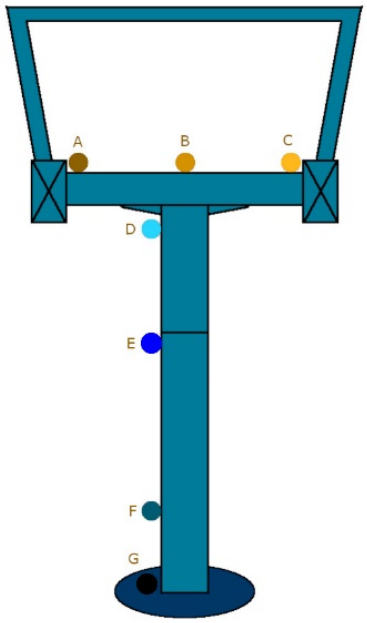




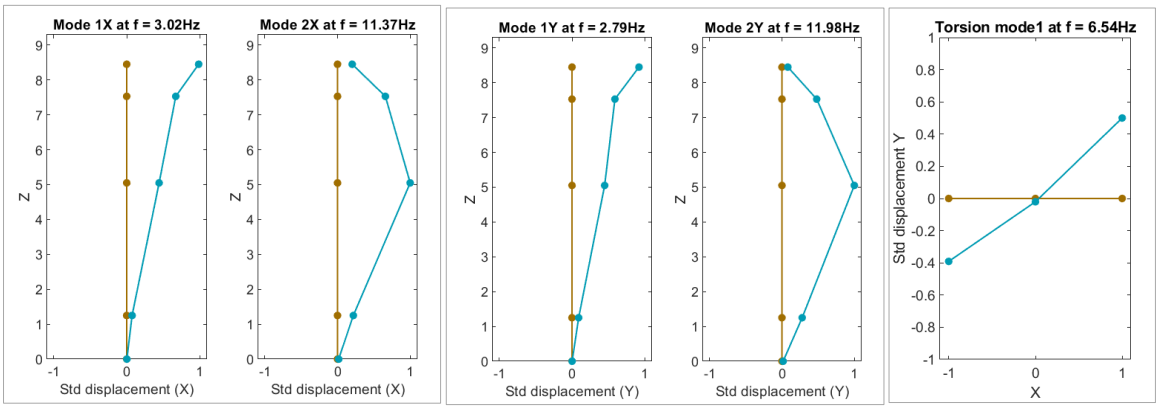
CARACTÉRISTIQUES DIMENSIONNELLES	
Diamètre des fils acier	2,8mm
Diamètre des fils Aluminium	2.8mm
Nombre de fil acier	7
Diametre du porteur central Acier	8,4mm
Diamètre du conducteur (mm)	19,6mm
Nombre de fils aluminium	30
Surface de l'acier	43,1mm²
Surface de l'aluminium ou de l'AGS	184,7mm²
Poids d'acier	342kg/km
Poids en aluminium	510kg/km
Masse approximative	856kg/km
Sens de la couche extérieure	S
CARACTÉRISTIQUES ÉLECTRIQUES	
Résistance ohmique max. du conducteur à 20°C	0,1805Ohm/km
CARACTÉRISTIQUES MÉCANIQUES	
Coefficient d'allongement	18,110E-6/°C
Charge de rupture minimale	120,8kN
Module d'élasticite (MPa)	84000
CARACTÉRISTIQUES D'UTILISATION	
Rayon de courbure en cours de pose	588mm

[6] Experimental reference results of tests on ski-lift tower with velocimeters

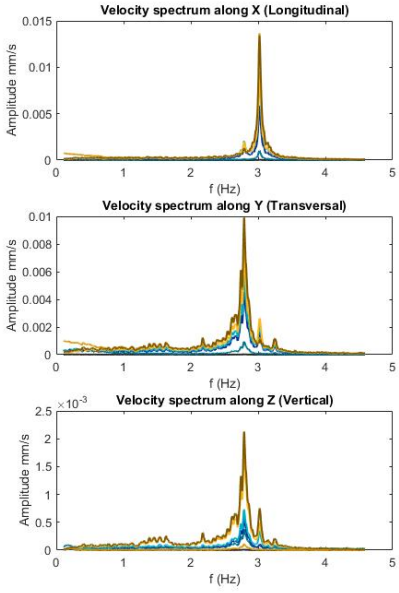




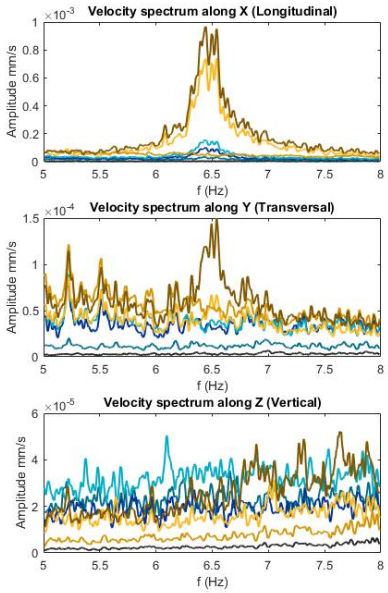
Semilog full frequency spectrum



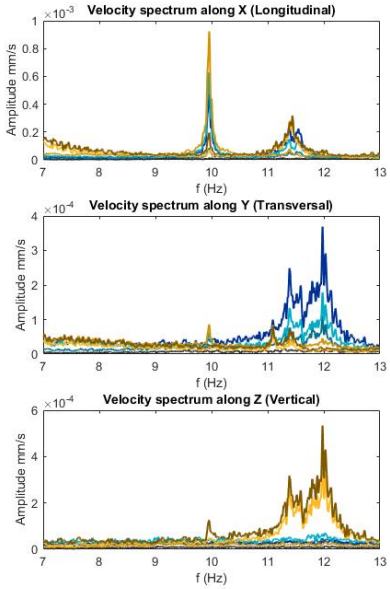
Deformed shape for the reference recording: no load applied, and all bolts screwed



First X & Y bending modes

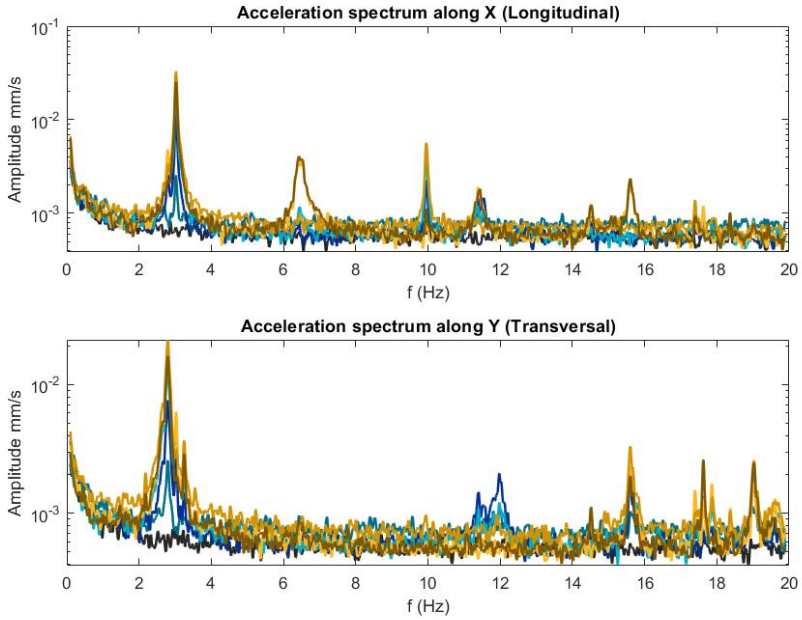


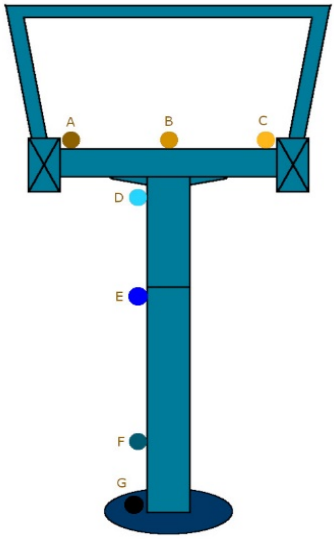
First torsion mode



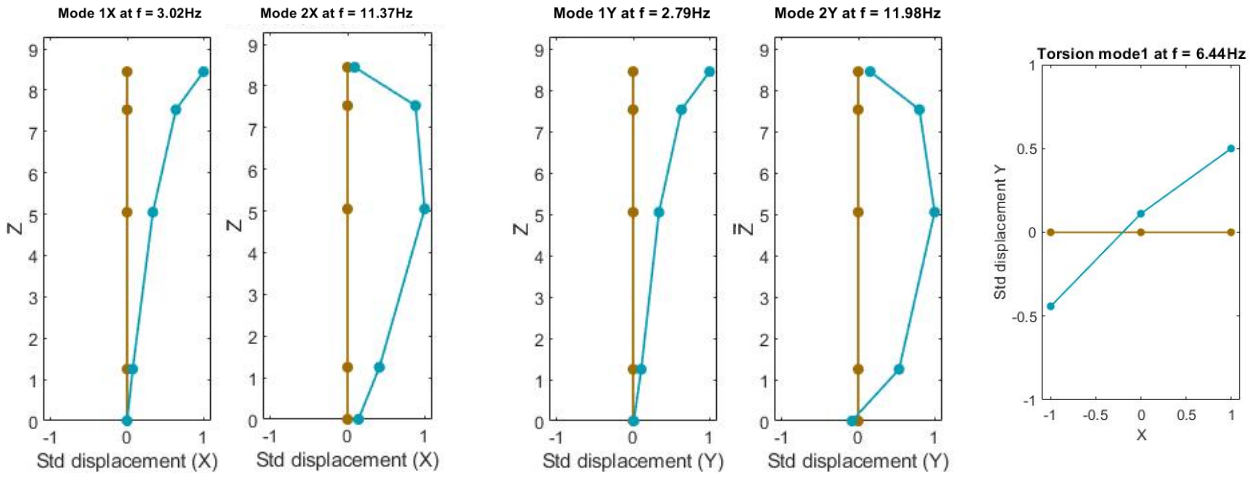
Second X & Y bending modes

[7] Experimental reference results of tests on ski-lift tower with MEMS accelerometers





Semilog frequency spectrum



Deformed shapes for the first bending & torsion modes

[8] Experimental results of tests on ski-lift tower with velocimeters in all configurations

Serie 8	Reference		
	Mode 1	Mode 2	Mode 3
Bending Y	2.79	11.38; 11.97	19.03
Bending X	3.01	9.96	11.38
Torsion	6.54	14.52; 15.61	

Serie 4	bilateral load + 50% unbolted on Y		
	Mode 1	Mode 2	Mode 3
Bending Y	1.81; 2.68	11.54; 12.21; 13.03	15.44
Bending X	1.80;2.69	9.96	
Torsion	6.43	11.53	14.61

Serie 1	one bolt unscrewed on X		
	Mode 1	Mode 2	Mode 3
Bending Y	2.64	12.09	
Bending X	2.64; 3.04	11.2	
Torsion	6.51		

Serie 5	unilateral load + 50% unbolted on Y		
	Mode 1	Mode 2	Mode 3
Bending Y	2.56; 2.90	12.35	15.4
Bending X	2.56; 2.90	9.95	
Torsion	6.46	11.56	

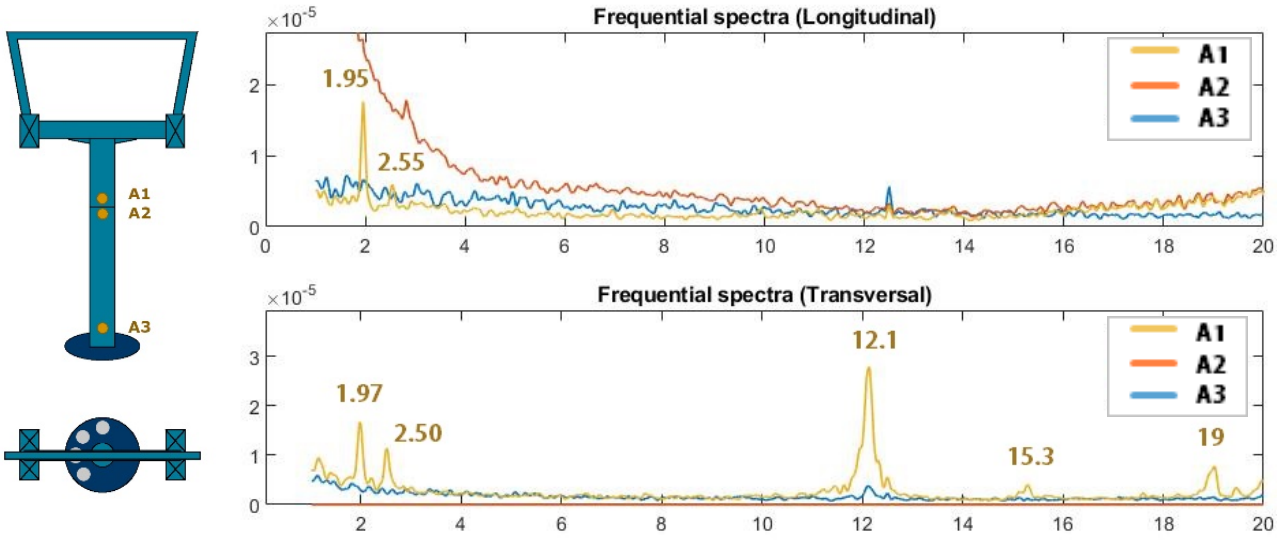
Serie 2	unilateral load		
	Mode 1	Mode 2	Mode 3
Bending Y	2.88; 3.13	11.51; 12.65	
Bending X	2.88; 3.13	9.97	14.57
Torsion	6.54	11.54	

Serie 6	50% unbolted on Y		
	Mode 1	Mode 2	Mode 3
Bending Y	1.57; 2.56	11.26; 11.73	
Bending X	1.57; 2.56	9.95	11.36
Torsion	6.45	15.6	

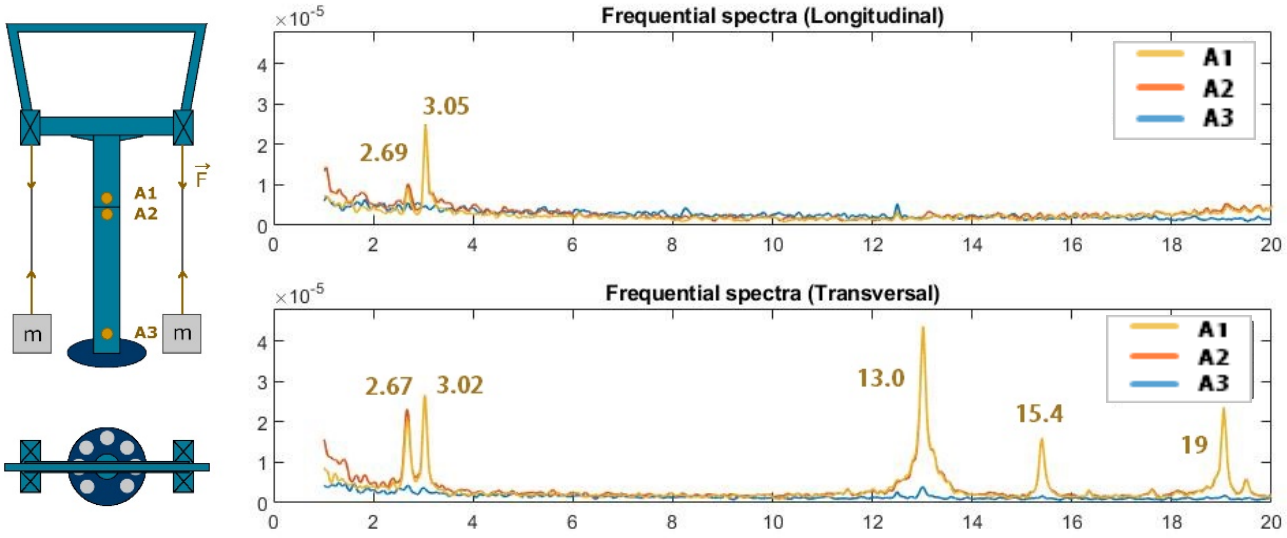
Serie 3	bilateral load		
	Mode 1	Mode 2	Mode 3
Bending Y	2.68; 3.06	11.59; 12.23; 13.14	15.49
Bending X	(2.69); 3.06	9.65; 9.99	
Torsion	6.52	11.58	

Serie 7	recording while screwing bolts (hitting)		
	Mode 1	Mode 2	Mode 3
Bending Y	2.73;2.83; 3.01	11.84	
Bending X	3.017		
Torsion			

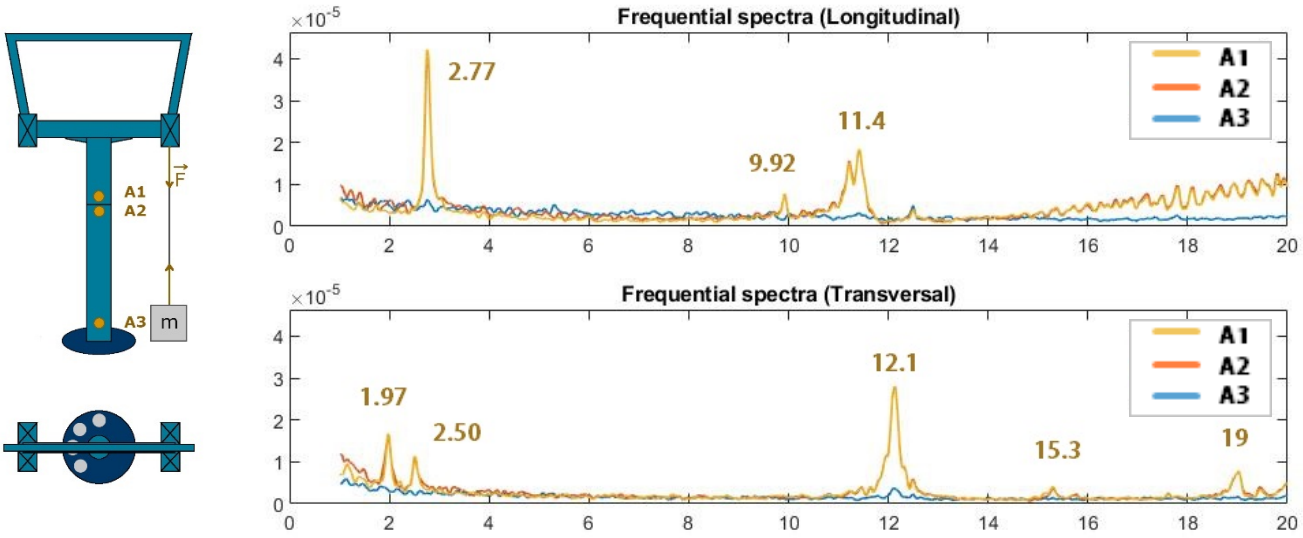
[9] Experimental results of piezo electric accelerometers in all configurations



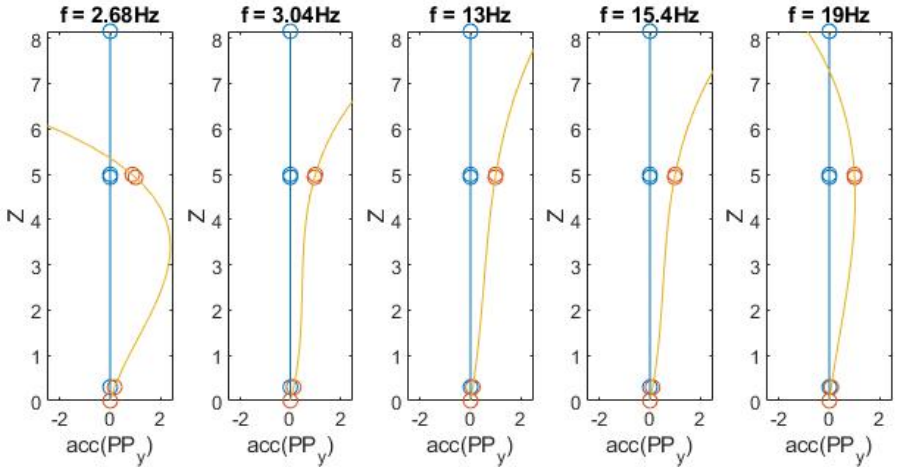
Frequency spectrum. 50% bolts screwed, load 1.5T on one side



Frequency spectrum. 90% bolts screwed, load 1.5T on both sides

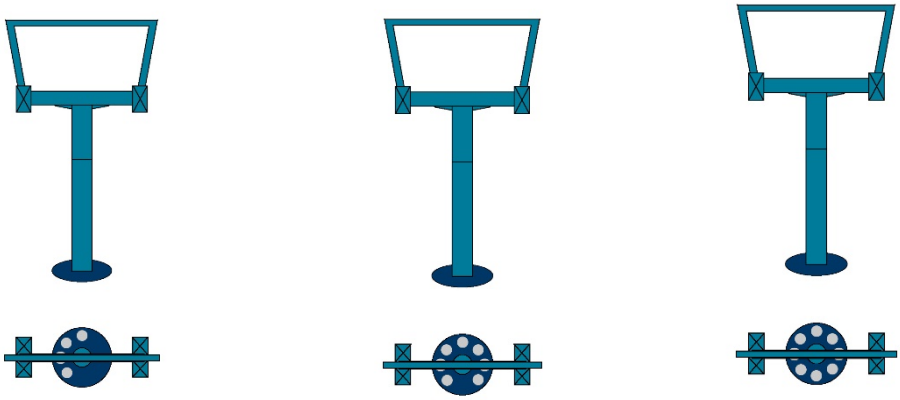


Frequency spectrum. 50% bolts screwed, no load



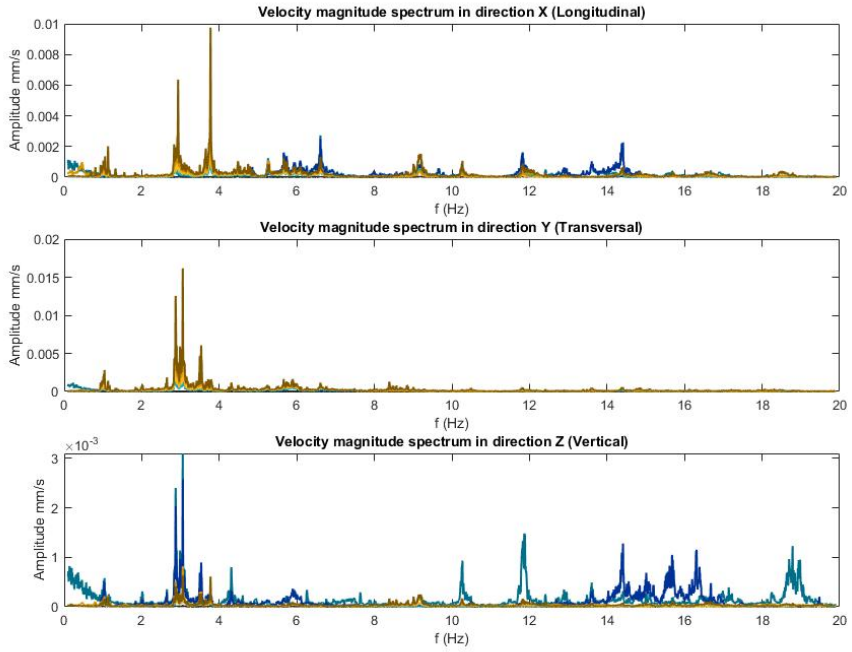
Example of a deformed shape built with spline interpolation/extrapolation. 50% bolts screwed, no load

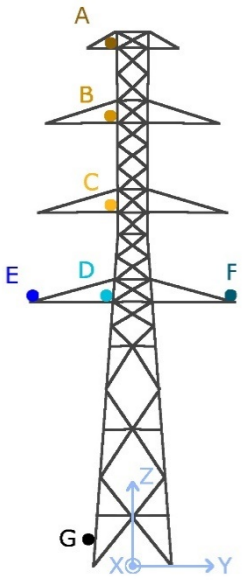
[10] Experimental results table for tests on the bolts of the ski-lift tower

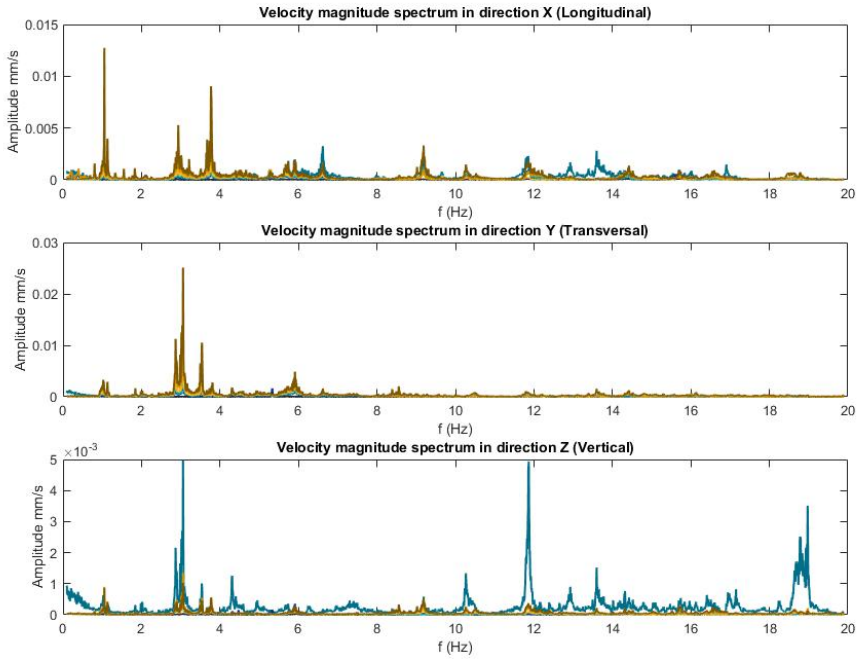


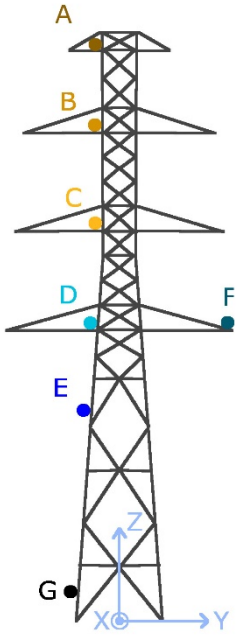
	50% bolts screwed		90% bolts screwed		100% bolts screwed
	Vel.	***Acc.***	***Vel.***	***Acc.***	***Vel.***
Mode 1X [Hz]	**2.55**	2.75	3.05	3.04	3.01
Mode 1Y [Hz]	**1.54**	2.39	2.64	2.67	2.79
Mode 2X [Hz]	11.36	11.39	11.47	11.51	11.43
Mode 2Y [Hz]	11.76	11.87	12.09	11.85	11.98
Mode 1T [Hz]	6.44	-	6.52	-	6.5
% f_0 for 1X	**85%**	91%	101%	101%	100%
% f_0 for 1Y	**55%**	86%	95%	96%	100%
% f_0 for 2X	99%	-	100%	-	100%
% f_0 for 2Y	98%	100%	101%	99%	100%
% f_0 for 1T	99%	-	100%	-	100%

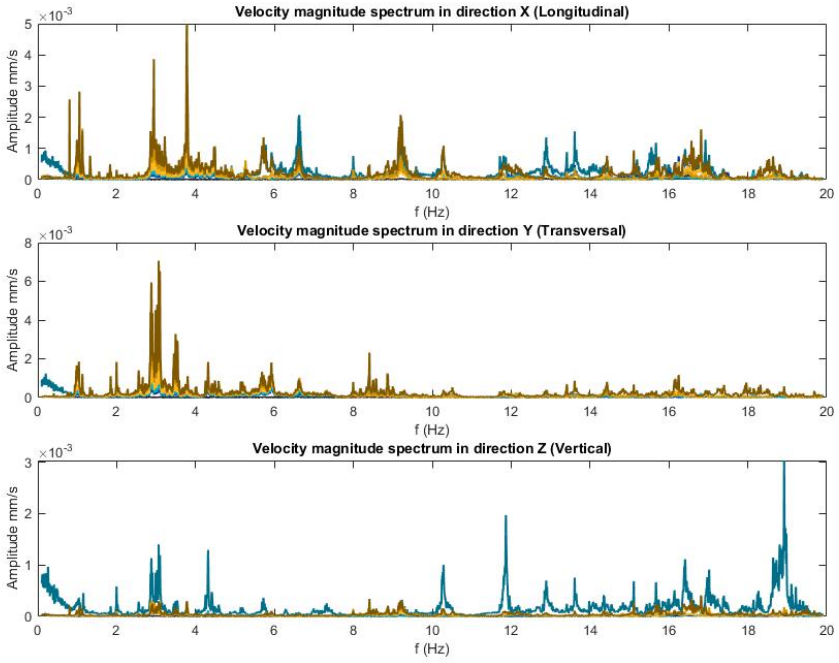
[11] Experimental spectra of tests on the power line tower

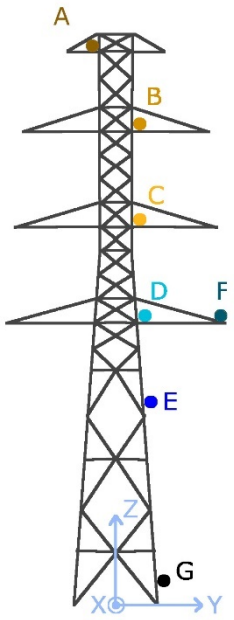


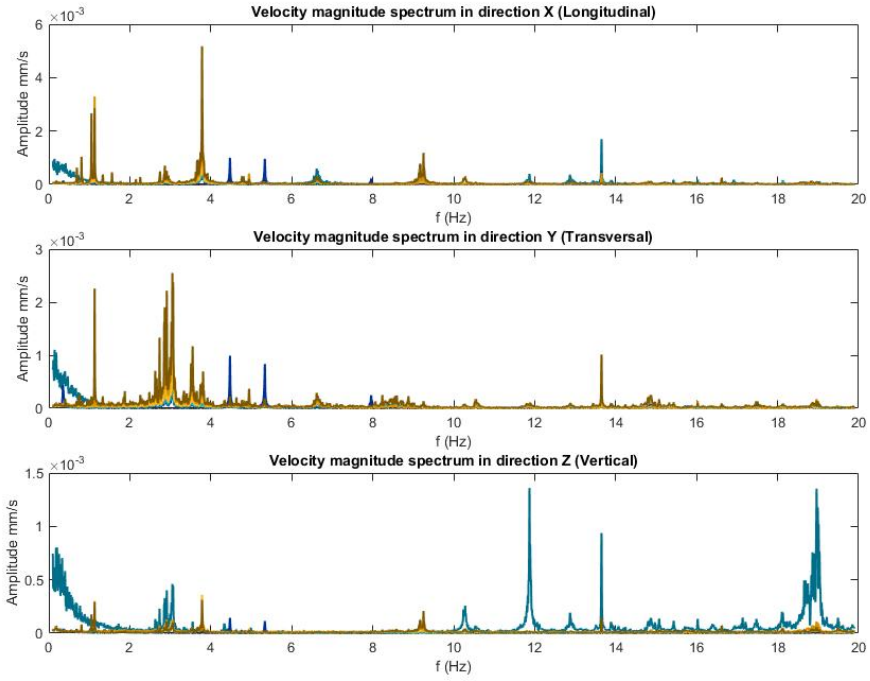


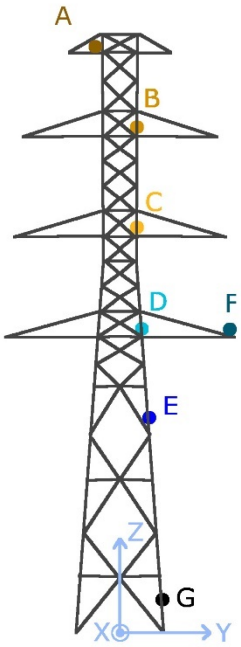


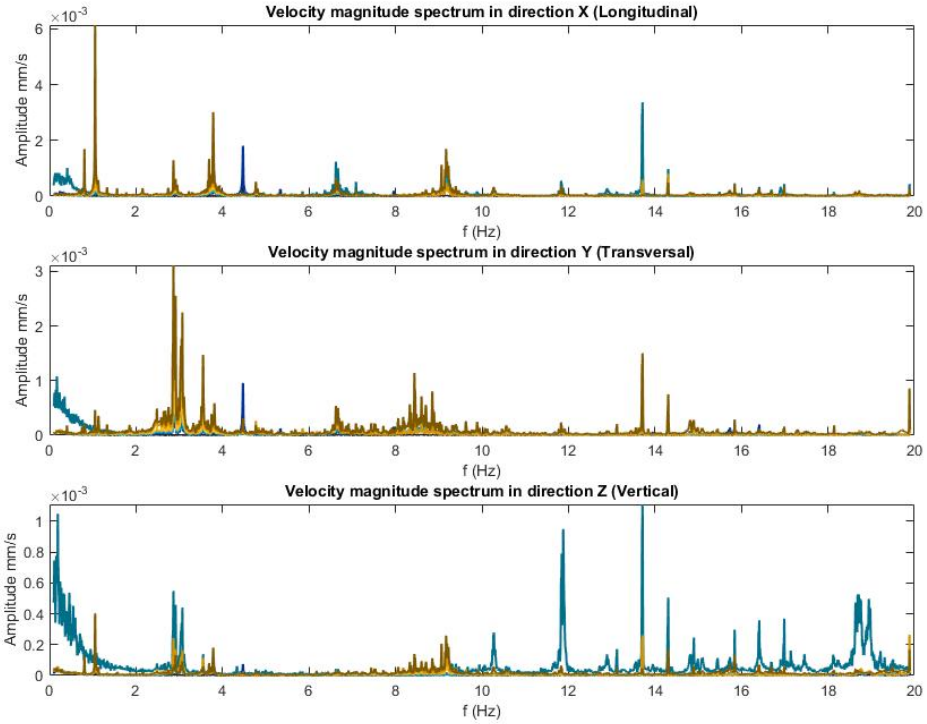


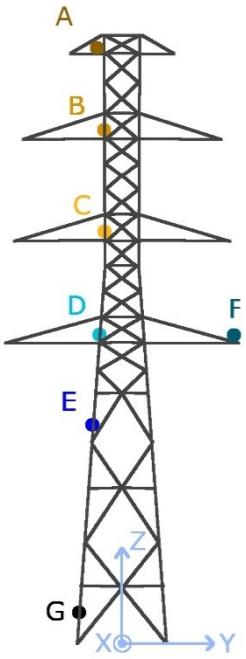

Velocity magnitude spectrum in direction X (Longitudinal)
Velocity magnitude spectrum in direction Y (Transversal)
Velocity magnitude spectrum in direction Z (Vertical)
Amplitude mm/s
f (Hz)


A
B
C
D
F
E
G
Z
X
Y

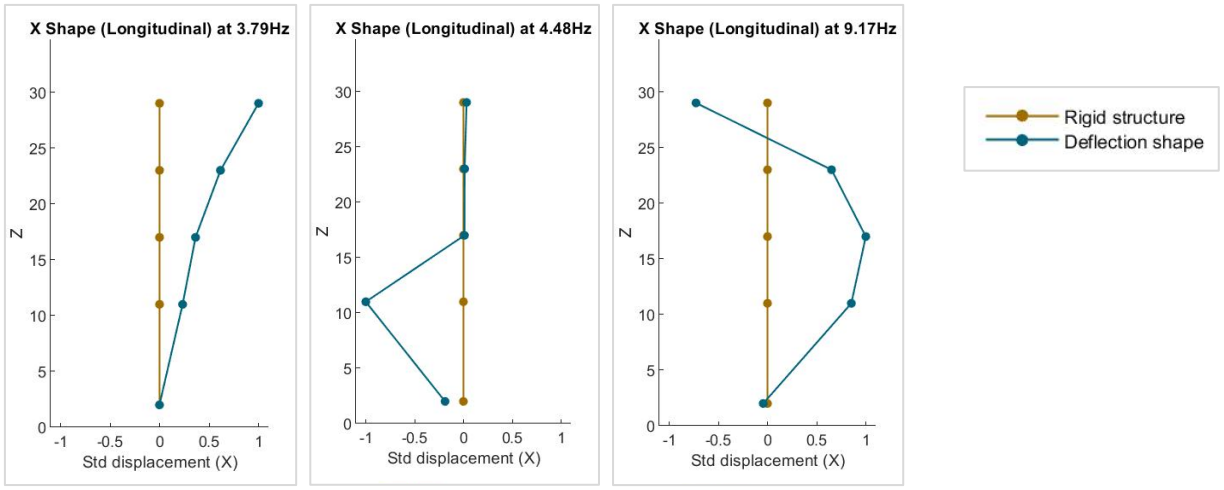

Velocity magnitude spectrum in direction X (Longitudinal)
Velocity magnitude spectrum in direction Y (Transversal)
Velocity magnitude spectrum in direction Z (Vertical)
Amplitude mm/s
f (Hz)


A
B
C
D
F
E
G
Z
X
Y

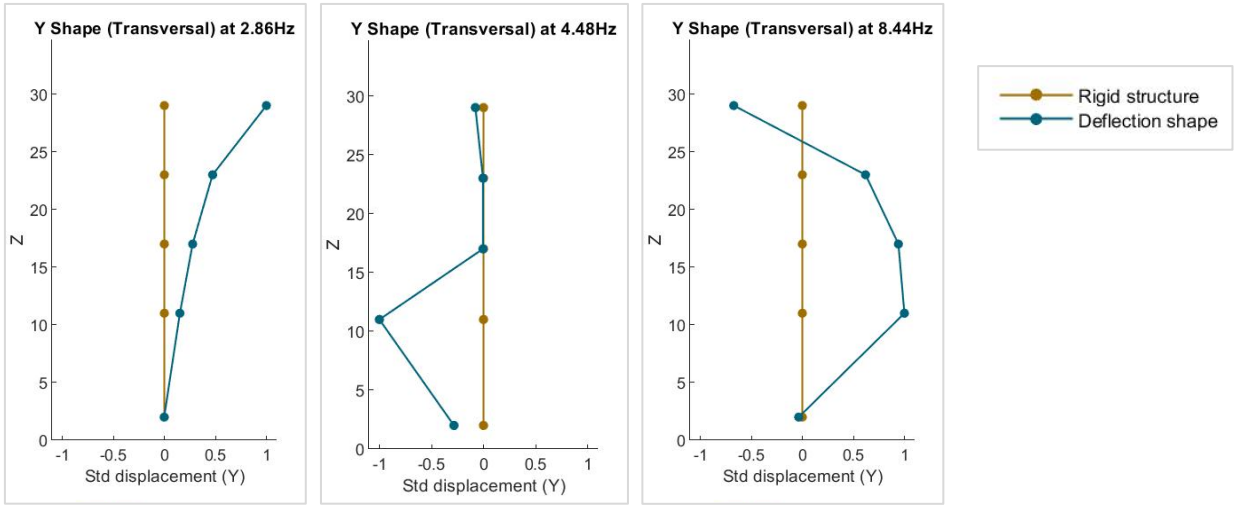

Velocity magnitude spectrum in direction X (Longitudinal)
Velocity magnitude spectrum in direction Y (Transversal)
Velocity magnitude spectrum in direction Z (Vertical)
Amplitude mm/s
f (Hz)
×10^-3


A
B
C
D
F
E
G
Z
X
Y

[12] Experimental deform shapes on the power line tower from velocimeters measurements

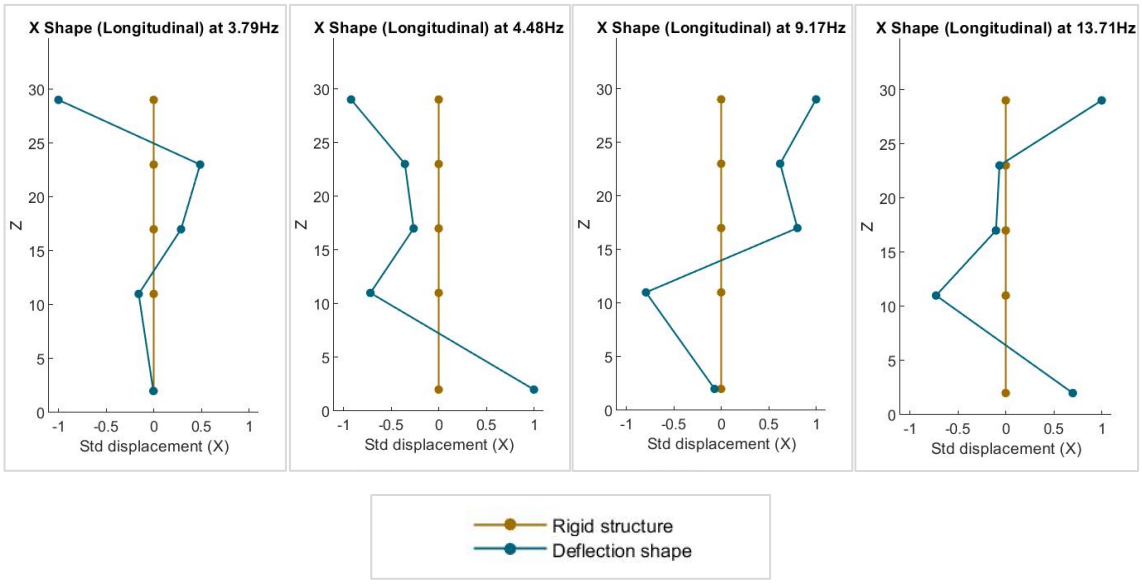


Mode shapes for every frequency peak along line direction (X)

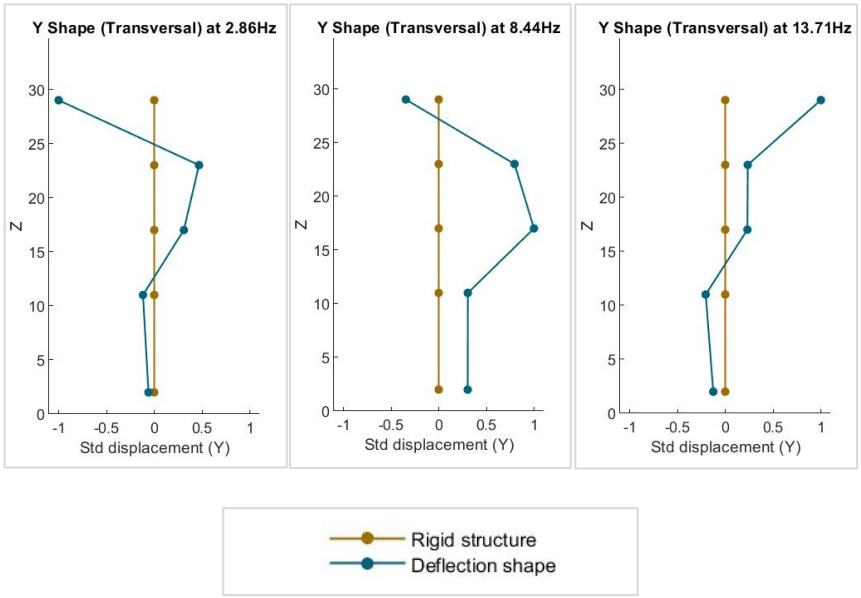


Mode shapes for every frequency peak perpendicular to line direction (Y)

[13] Experimental deform shapes on the power line tower from MEMS accelerometers measurements

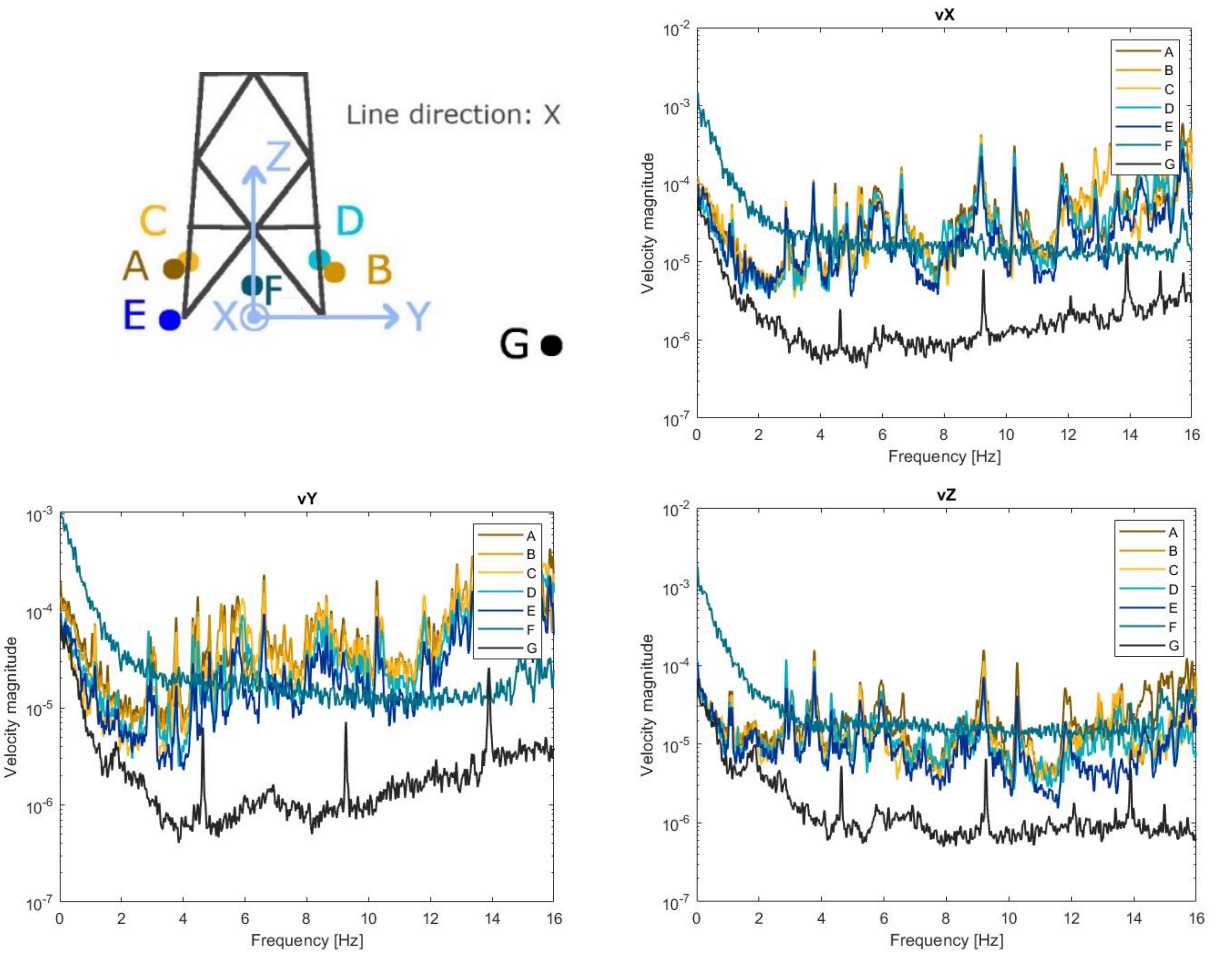


Mode shapes for every frequency peak along line direction (X)



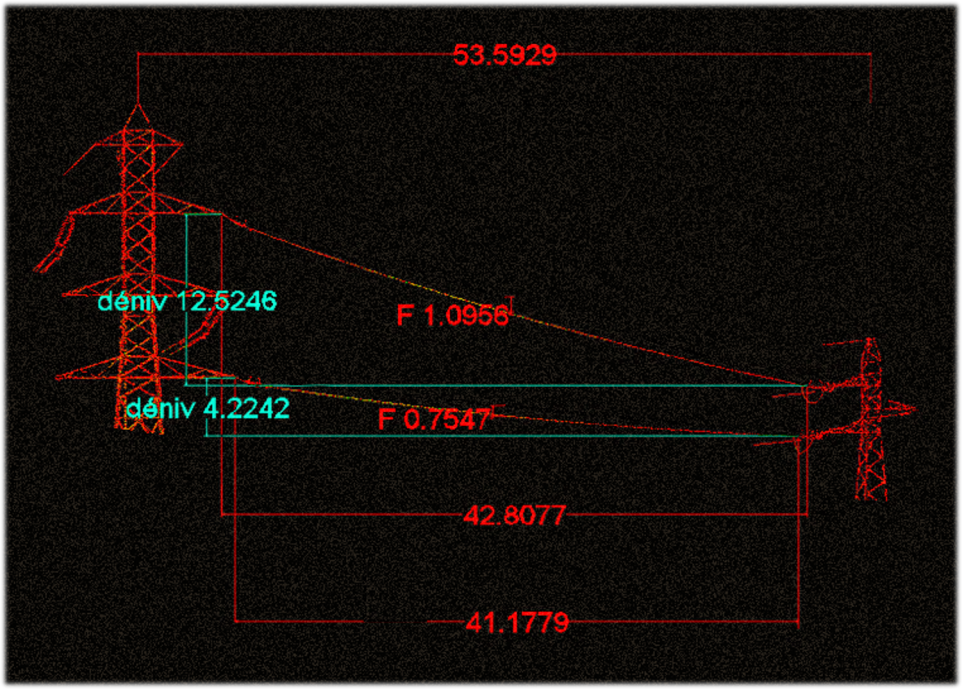
Mode shapes for every frequency peak perpendicular to line direction (Y)

[14] Experimental results of tests on power line tower regarding interaction soil-structure

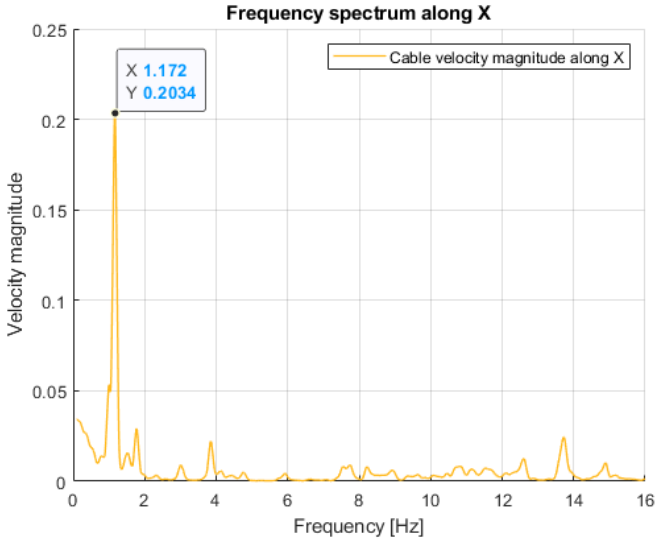


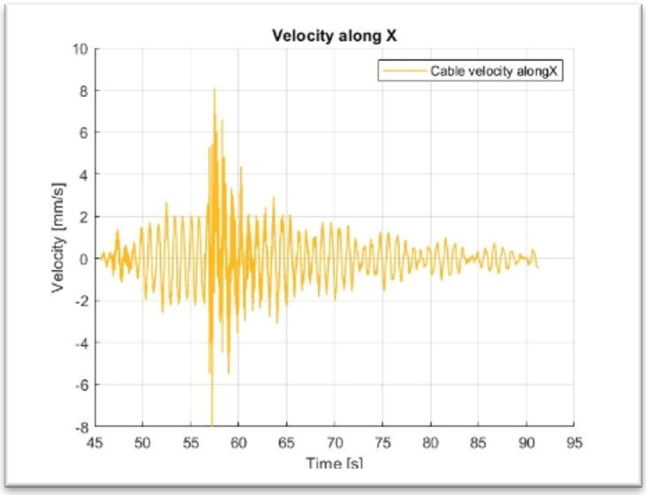
Disposition of the sensors and related semilog frequency spectra

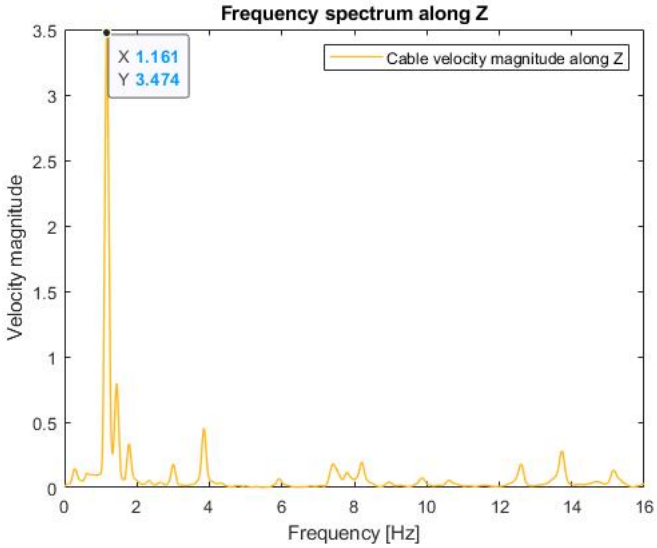
[15] Laser scanning of power line cables fixed on G4S1R1 tower

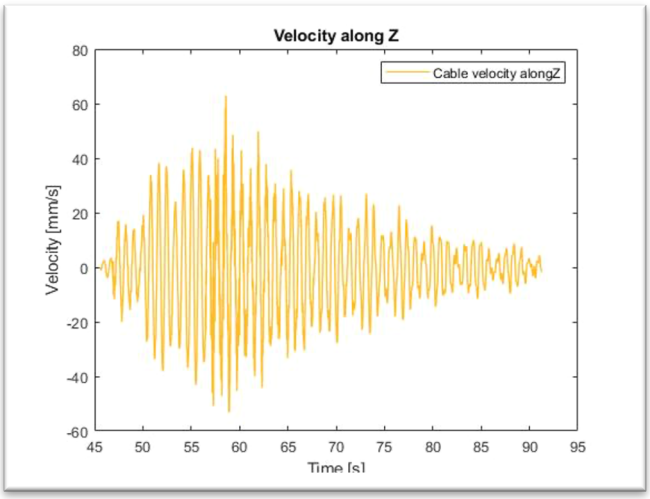


[16] Experimental results of tests on a high voltage cable

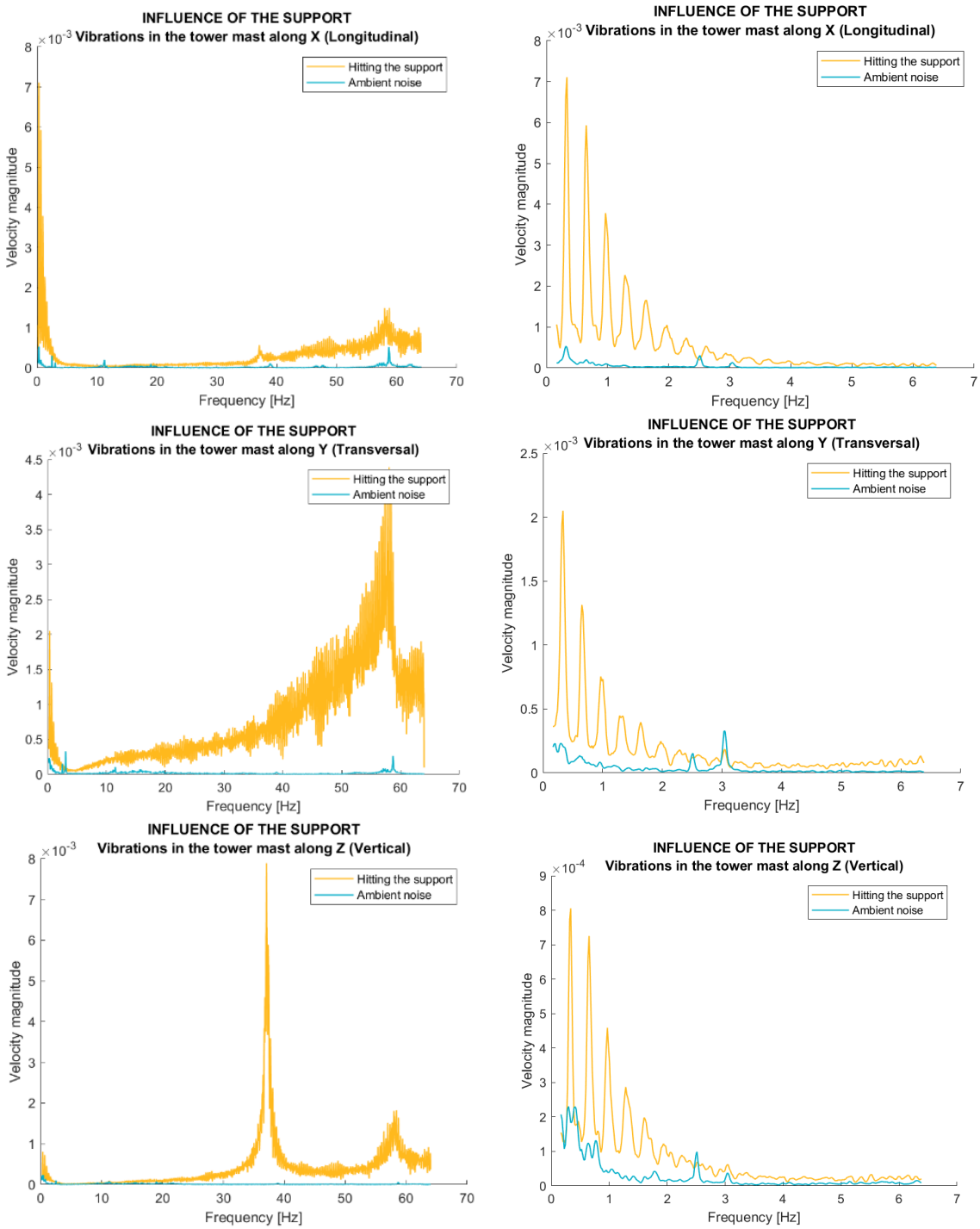








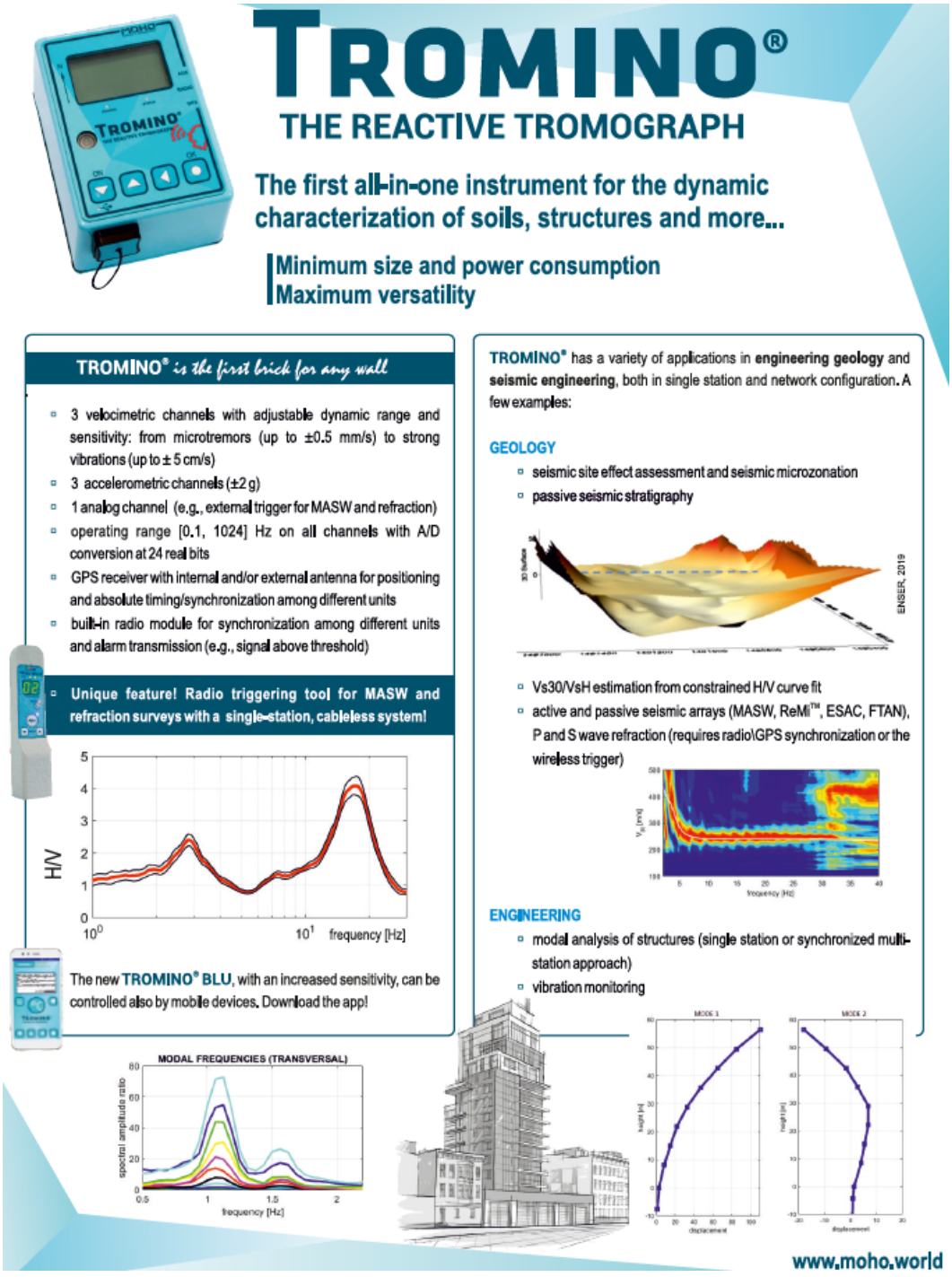
[17] Bracket resonance spectra



[18] **SURICAT® velocimeters (+ 3D MEMS accelerometers) by MOHO®, datasheet**



[19] **TROMINO® Premium 3D velocimeters (+ 3D MEMS accelerometers) by MOHO®, datasheet**



[20] Wired Low frequency accelerometers high sensibility WILCOXON®

Wilcoxon SENSING TECHNOLOGIES

Low-frequency, filtered accelerometer

799LF

SPECIFICATIONS

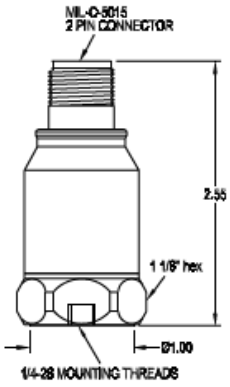
Sensitivity, ±5%, 25°C		500 mV/g
Acceleration range		10 g peak
Amplitude nonlinearity		1%
Frequency response:	±5%	0.3 - 1,200 Hz
	±10%	0.2 - 1,600 Hz
	±3 dB	0.1 - 2,500 Hz
Resonance frequency		18 kHz
Transverse sensitivity, max		5% of axial
Temperature response:	–50°C	–7%
	+120°C	+5%
Power requirement:		
Voltage source		15 - 30 VDC
Current regulating diode		2 - 10 mA
Electrical noise, equiv. g:		
Spectral	0.1 Hz	15 µg/√Hz
	1 Hz	3 µg/√Hz
	10 Hz	1 µg/√Hz
	100 Hz	1 µg/√Hz
Output impedance, max		400 Ω
Bias output voltage		8.0 VDC
Grounding		case isolated, internally shielded
Temperature range		–50° to +120°C
Vibration limit		250 g peak
Shock limit		5,000 g peak
Electromagnetic sensitivity, equiv. g		150 µg/gauss
Sealing		hermetic
Base strain sensitivity, max		0.0005 g/µstrain
Sensing element design		PZT ceramic / shear
Weight		205 grams
Case material		316L stainless steel
Mounting		1/4-28 tapped hole
Output connector		2 pin, MIL-C-5015 style
Mating connector		R6 type

Accessories supplied: SF6 mounting stud; calibration data (level 3)



Key features

- Ultra low noise
- Optimized for 15 V supply
- Available with M12 connector
- Manufactured in ISO 9001 facility





PIN-OUT

Connections	
Function	Connector pin
power/signal	A
common	B
ground	shell

CE

Note: Due to continuous process improvement, specifications are subject to change without notice.
This document is cleared for public release.

Wilcoxon Sensing Technologies
An Amphenol Company
98270 Rev.4 09/18

8435 Progress Drive
Frederick, MD 21701
USA

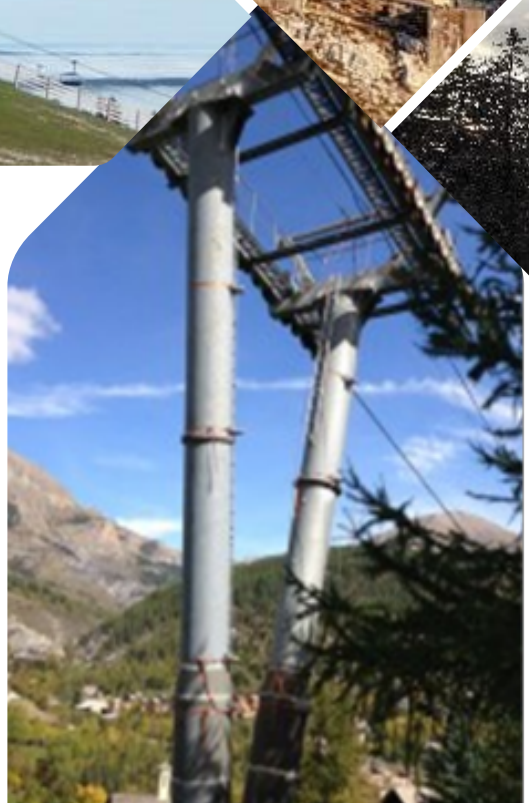
Tel: +1 (301) 330-8811
Fax: +1 (301) 330-8873
info@wilcoxon.com

buy.wilcoxon.com
www.wilcoxon.com









SARRASOLA
74, rue de la Gare
73460 GRESY SUR ISERE
T. + 33 (0) 4 79 37 94 16 - F. + 33 (0) 4 79 37 94 00

SARRASOLA – Entreprise du groupe VINCI ENERGIES

Société par action simplifiée au capital de 303 000 €

74, rue de la Gare –

73460 GRESY SUR ISERE